

Article

A Study on the Structure, Optical Properties and Cellular Localization of Novel 1,3-Benzothiazole-Substituted BODIPYs

Olga Kirkilessi ¹, Christina Arapatzi ², Heribert Reis ¹, Vassiliki Kostourou ² , Kyriakos C. Prousis ^{1,*}  and Theodora Calogeropoulou ^{1,*} 

¹ Institute of Chemical Biology, National Hellenic Research Foundation, 48 Vassileos Constantinou Avenue, 11635 Athens, Greece; okirkilessi@eie.gr (O.K.); hreis@eie.gr (H.R.)

² Institute for Bioinnovation, “Alexander Fleming” Biomedical Sciences Research Center, 34 Fleming Str. Vari, 16672 Athens, Greece; arapatzi@fleming.gr (C.A.); kostourou@fleming.gr (V.K.)

* Correspondence: kyrprousis@eie.gr (K.C.P.); tcalog@eie.gr (T.C.)

Abstract: A library of seven novel 1,3-benzothiazole-substituted BODIPY derivatives with tunable optical properties was synthesized. The new fluorescent dyes exhibited bathochromically shifted absorptions (up to 670 nm) and emissions centered in the red and near-infrared spectral region (up to 677 nm) in comparison to the parent compound 8-phenyl BODIPY (λ_{abs} : 499 nm, λ_{emi} : 508 nm). (TD)DFT calculations were performed to rationalize the spectroscopic properties of the new dyes. The cellular biodistribution of the new BODIPY dyes, their fluorescence stability and toxicity were investigated in both living and fixed fibroblasts using time-lapse fluorescent imaging and confocal microscopy. Six of the seven new dyes were photostable and non-toxic in vitro at 10 μM concentration. In addition, they efficiently stained the cell membrane, showing diffuse and dotted localization within the cell at low concentrations (1.0 and 0.1 μM). Specifically, dye **TC498** was localized in vesicular structures in both live and fixed cells and could be used as a suitable marker in co-staining studies with other commonly used fluorescent probes.

Keywords: BODIPYs; synthesis; DFT calculation; cellular biodistribution; time-lapse fluorescent imaging; confocal microscopy



Citation: Kirkilessi, O.; Arapatzi, C.; Reis, H.; Kostourou, V.; Prousis, K.C.; Calogeropoulou, T. A Study on the Structure, Optical Properties and Cellular Localization of Novel 1,3-Benzothiazole-Substituted BODIPYs. *Colorants* **2024**, *3*, 17–38. <https://doi.org/10.3390/colorants3010002>

Academic Editor: Aleksander Filarowski

Received: 15 October 2023

Revised: 15 December 2023

Accepted: 20 December 2023

Published: 31 December 2023



Copyright: © 2023 by the authors. Licensee MDPI, Basel, Switzerland. This article is an open access article distributed under the terms and conditions of the Creative Commons Attribution (CC BY) license (<https://creativecommons.org/licenses/by/4.0/>).

1. Introduction

Borondipyrromethenes (BODIPYs) constitute a privileged class of organic fluorophores with applications in various biomedical fields [1–3]. They are used for fluorescence sensing [4,5] and fluorescence imaging [6–9], as photosensitizers in photodynamic [10–14] and photothermal therapy [15], and more recently, they have been explored in photoacoustic imaging [16–18]. BODIPYs are functional dyes exhibiting strong absorption and narrow emission peaks between the visible and the near-infrared region, Ref. [19] moderate Stokes shifts, high fluorescence quantum efficiency [20–22] and insensitivity to polarity and pH [23,24]. In general, they are chemically stable, have the ability to cross the cell membrane since they are not charged, and easily accumulate in subcellular organelles due to their comparatively high hydrophobicity [25–27]. However, fine-tuning of lipophilicity is required depending on the specific biolabeling application [28]. BODIPY dyes tend to aggregate in aqueous solutions and have a tendency to concentrate in lipophilic compartments in cells, which may result in non-specific staining of cell membranes and other organelles [29,30]. Hence, to increase hydrophilicity and reduce non-specific fluorescence, the BODIPY scaffold has been decorated with a variety of polar groups [31–33].

It is well known that the emissive behavior of BODIPY fluorophores is greatly influenced by the steric and electronic effects of their substituents [34]. The free rotation or rigidity of the various structural components, as well as their electron-donating or withdrawing properties, greatly influence the brightness, the absorptive and the emissive properties of BODIPY dyes [35]. The BODIPY scaffold can be functionalized through simple

chemical modifications at the meso-, α -, β - positions and at the B(III) center by introducing various substituents, thus rigidifying the structure and fine-tuning the optical properties and biocompatibility of the final dyes (Figure 1) [36].

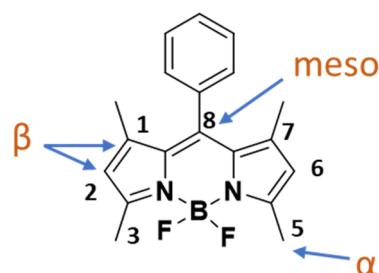


Figure 1. Positions for the potential modifications on the BODIPY scaffold.

Despite the synthesis of various BODIPY derivatives [8,35–37] that address specific bioimaging requirements [2], a number of drawbacks characteristic of these dyes have not been resolved satisfactorily to date. In particular, the majority of BODIPYs emit at wavelengths lower than 600 nm, interfere with other commonly used fluorescent dyes and cause autofluorescence background and light-scattering. Additionally, their highly conjugated structure makes them extremely lipophilic, which favors aggregation, thus impeding membrane permeability [29]. Therefore, there is a continuous need for custom-made dyes with fine-tuned properties that meet specific demands for bioimaging applications *in vitro* and *in vivo*.

1,3-benzothiazole (BZT) is a biologically important heterocycle with metabolic stability, decreased cytotoxicity and excellent cell permeability and is encountered in various bioactive compounds [38]. Furthermore, BZT has been used as a substitute in various fluorescent dyes [39], including cyanine dyes [40], pyronin dyes [41] and hetarylazopyrazolone dyes [42]. Benzothiazole-based fluorescent probes have several advantages, including high quantum yields, large Stoke shifts and high molar extinction coefficients, and have been investigated in the diagnosis of a number of disorders using imaging modalities [43]. The most widely used among the benzothiazole-based fluorophores are the 2-(2-hydroxyphenyl) benzothiazole (HBT) and thiazole orange (TO) (Figure 2).

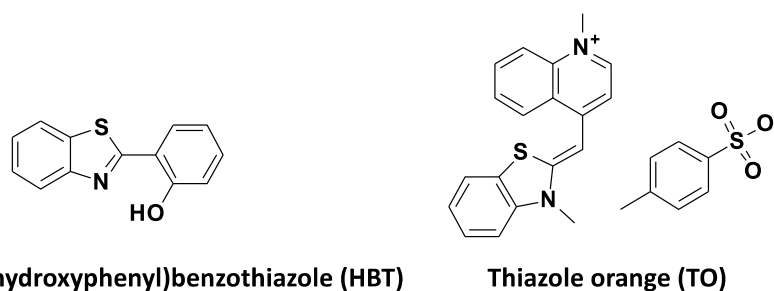


Figure 2. Structures of 2-(2-hydroxyphenyl) benzothiazole (HBT) and thiazole orange (TO).

Regardless of the broad applicability of the BZT moiety in the development of new fluorescent dyes, this heterocycle has been scarcely explored in conjunction with the BODIPY core. Recently, Shi et al. reported the synthesis of a meso-BZT-substituted BODIPY-based aggregation-induced emission (AIE) fluorescent rotor that was used in monitoring autophagy and imaging lysosomal viscosity [44] (Figure 3). Furthermore, Poronik et al. prepared three bis(1,3-benzothiazolyl)-substituted BODIPY dyes that possessed emission wavelengths ~640 nm, moderate molar extinction coefficients and intense fluorescence [45] (Figure 3). Finally, Sansalone et al. sought to investigate the conformational isomers with antiperiplanar and periplanar arrangements of BODIPY chromophores connected to a benzoxazole, benzothiazole or nitrobenzothiazole through an olefinic bridge with *trans* configuration [46] (Figure 3).

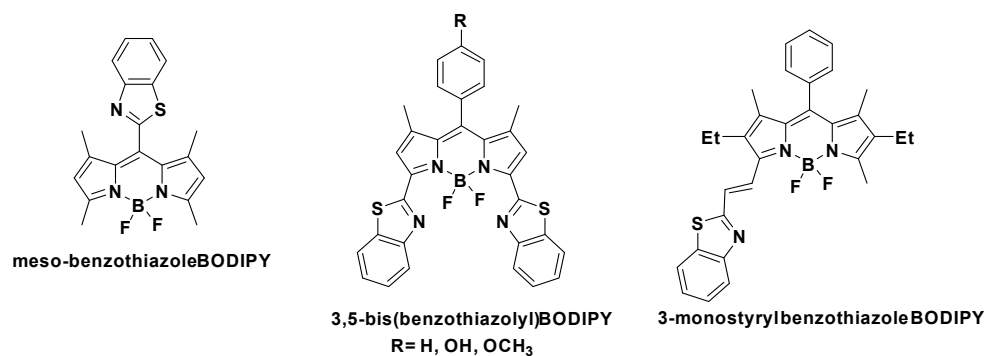


Figure 3. Structures of known BZT-substituted BODIPY dyes.

In the context of our studies on the synthesis of new fluorophores [47], recognizing the need for improved BODIPY derivatives for biomedical applications and intrigued by the interesting properties endowed in fluorescent probes by the BZT moiety, we set out to perform a more detailed study on BZT-substituted BODIPYs. Thus, a library of six BZT-substituted BODIPYs was prepared through modifications of 8-phenyl BODIPY at C3, C5 and C6 (TC495–TC498, TC500 and TC514). In addition, the congener of TC514, dye TC516, in which the phenyl group at the meso position was replaced by the BZT moiety, was synthesized (Figure 4). The photophysical characterization of the new dyes was supplemented by (TD)DFT calculations to rationalize their optical properties. Moreover, the cellular localization of the new dyes, their fluorescence stability, spectral properties and toxicity were studied in both living and fixed fibroblasts using time-lapse fluorescent imaging and confocal microscopy.

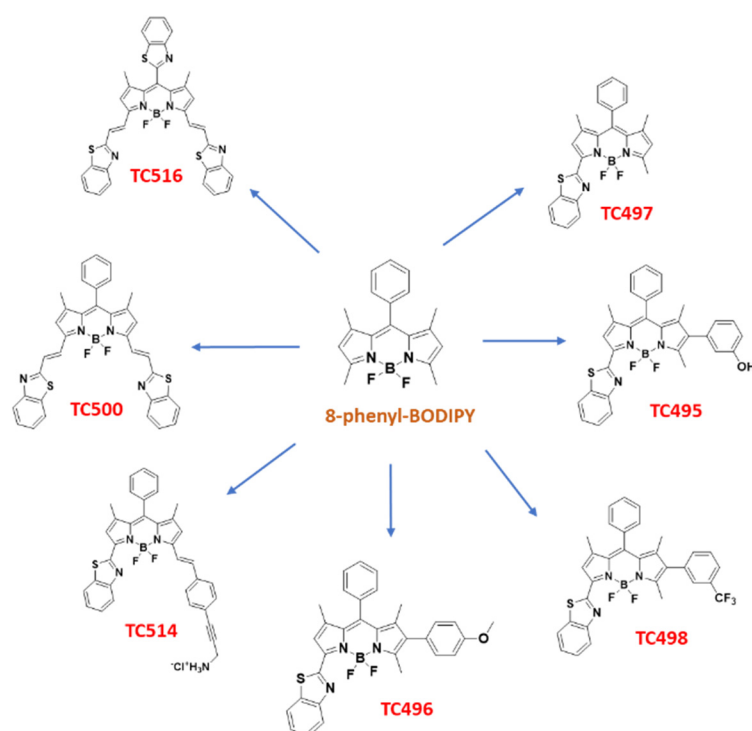


Figure 4. Structures of the novel synthesized BZT-substituted BODIPY dyes of the present study.

2. Materials and Methods

2.1. General Information for Synthesis

All reactions were carried out under scrupulously dry conditions. THF was distilled over sodium in the presence of benzophenone, and DCM was distilled over calcium hydride. NMR spectra were recorded on Varian spectrometers (Varian, Palo Alto, CA, USA). ¹H

NMR spectra were recorded at 600 or 300 MHz, ^{13}C NMR spectra at 150.9 or 75.5 MHz, and were internally referenced to residual solvent signals. Data for ^1H NMR are reported as follows: chemical shift (δ ppm), multiplicity (s = singlet, bs = broad singlet, d = doublet, t = triplet, m = multiplet), coupling constant, and integration. Data for ^{13}C NMR are reported in terms of chemical shift (δ ppm). High-resolution mass spectra were recorded on a UHPLC LC-MSⁿ Orbitrap Velos-Thermo instrument (Thermo Scientific Waltham, MA, USA). Thin-layer chromatography (TLC) was carried out on pre-coated silica gel (0.2 mm, 60 F254) glass plates (Merck KGaA, Darmstadt, Germany). Chromatographic purification was performed by flash column chromatography (FCC) using silica gel (200–400 mesh) (Merck KGaA, Darmstadt, Germany). Steady-state UV-Vis electronic absorption spectra were recorded on a Lambda 19 UV-Vis-NIR spectrophotometer (Perkin Elmer, Beaconsfield, UK). Steady-state emission spectra were recorded on a GL3-21 spectrofluorometer (Horiba Fluorolog-3 JobinYvon-Spex, Oberursel, Germany). Pico-second time-resolved fluorescence spectra were measured by the time-correlated-single-photon-counting (TCSPC) method on a Nano-Log spectrofluorometer (Horiba JobinYvon, Oberursel, Germany) by using a laser diode as an excitation source (NanoLED, 654 and 784 nm) and a UV-Vis detector TBX-PMT series (250–850 nm) (Horiba JobinYvon, Oberursel, Germany). Lifetimes were evaluated with the DAS6 Fluorescence-Decay Analysis Software. Melting points were obtained with an ET0001 Electrothermal Digital Melting Point Apparatus, (Cole-Parlmer, Vernon Hills, IL, USA), and are uncorrected.

2.2. Synthetic Procedures

2.2.1. Synthesis of 8-Phenyl-BODIPY (1)

8-phenyl-BODIPY (1) was prepared as described in the literature [48]. Briefly, to a solution of benzaldehyde (0.25 mL, 2.5 mmol) and 2,4-dimethyl-1H-pyrrole (0.65 mL, 6.25 mmol) in dry dichloromethane (DCM) (75 mL), trifluoroacetic acid (TFA) (25 μL , 0.33 mmol) was added dropwise, and the mixture was stirred for 3 h. The reaction mixture was cooled at 0 °C and a solution of 2,3-dichloro-5,6-dicyano-1,4-benzoquinone (DDQ) (567 mg, 2.5 mmol) in dry DCM (45 mL) was added over 1 h. Subsequently, Et_3N (5 mL, 36 mmol) was added, followed by the addition of $\text{BF}_3 \cdot \text{Et}_2\text{O}$ (5 mL, 40 mmol) at room temperature (RT). After stirring for 20 min, the reaction was quenched with H_2O . The two layers were separated, and the organic layer was washed with H_2O (3 \times 100 mL), dried over anhydrous Na_2SO_4 and concentrated under reduced pressure. The brown oily residue was purified by FCC (elution system: petroleum ether (PE) 40–60 °C/ethyl acetate (EtOAc) 98:2) to afford 8-phenyl-BODIPY (1) as a red-yellowish solid (397 mg, 49% yield). R_f : 0.33 (PE 40–60 °C/EtOAc 97:3); ^1H NMR (600 MHz, CDCl_3): δ 7.47–7.50 (m, 3H), 7.27–7.29 (m, 2H), 5.98 (s, 2H), 2.56 (s, 6H), 1.37 (s, 6H).

2.2.2. Synthesis of 3-(8-Phenyl-BODIPY)-Carbaldehyde (2)

To a degassed solution of 8-phenyl-BODIPY (1) (110 mg, 0.34 mmol) in EtOAc (15 mL), pyridinium chlorochromate (PCC) (438.8 mg, 2.03 mmol) was added and the reaction mixture was stirred at RT for 12 h. Upon completion of the reaction, the mixture was filtered through a silica gel pad using EtOAc (60 mL) as eluent. The filtrate was evaporated under reduced pressure, and the residue was purified by FCC (elution system: PE 40–60 °C/EtOAc 9:1) to afford aldehyde 2 as a yellow solid (77 mg, 67% yield). R_f : 0.65 (PE 40–60 °C/EtOAc 7:3); m.p. 214–216 °C; ^1H NMR (600 MHz, CDCl_3): δ 10.28 (s, 1H, CHO), 7.56–7.53 (m, 3H), 7.32–7.30 (m, 2H), 6.78 (s, 1H), 6.23 (s, 1H), 2.67 (s, 3H), 1.47 (s, 3H), 1.40 (s, 3H); ^{13}C NMR (600 MHz, CDCl_3): δ 184.6, 166.2, 149.9, 144.1, 138.0, 134.0, 129.8, 129.7, 127.8, 127.6, 125.3, 120.2, 119.9, 15.8, 15.1, 14.2; HRMS (ESI⁺) Found: $[\text{M}+\text{H}]^+$ 339.1478; molecular formula $\text{C}_{19}\text{H}_{18}\text{ON}_2\text{BF}_2$ requires $[\text{M}+\text{H}]^+$ 339.1475.

2.2.3. Synthesis of 3-(Benzo[d]Thiazol-2-yl)-8-Phenyl-BODIPY (TC497)

To a solution of 2 (20 mg, 0.06 mmol) in anhydrous dimethylformamide (DMF) (0.97 mL), 1,2-aminothiophenol (9 μL , 0.09 mmol) and *p*-toluenesulfonic acid (TsOH) (2 mg,

0.012 mmol) were added and the reaction mixture was stirred at 72 °C for 12 h. Upon completion of the reaction, DCM and water were added to the reaction mixture, and the organic phase was separated and washed with brine (3 × 30 mL), dried over anhydrous Na₂SO₄ and concentrated on a rotary evaporator. The residue was purified by FCC (elution system: PE 40–60 °C/EtOAc 9:1 to 8:2) to obtain dye **TC497** as a pink-orange solid (13 mg, 52% yield). *R*_f: 0.68 (PE 40–60 °C/EtOAc 7:3); m.p. 198–200 °C; ¹H NMR (600 MHz, CDCl₃): δ 8.12 (d, *J* = 8.2 Hz, 1H), 7.93 (d, *J* = 8.0 Hz, 1H), 7.52–7.54 (m, 3H), 7.50 (t, *J* = 7.7 Hz, 1H), 7.40 (t, *J* = 7.6 Hz, 1H), 7.32–7.37 (m, 2H), 7.12 (s, 1H), 6.14 (s, 1H), 2.67 (s, 3H), 1.46 (s, 3H), 1.45 (s, 3H); ¹³C NMR (150 MHz, CDCl₃): δ 161.5, 158.8, 153.0, 147.0, 144.4, 143.1, 140.3, 139.4, 137.1, 137.0, 134.7, 134.0, 133.4, 129.5, 128.0, 126.4, 125.7, 123.9, 123.5, 123.4, 121.6, 114.2, 15.4, 14.8, 14.5; HRMS (APCI⁺) Found: [M+H]⁺ 444.1515; molecular formula C₂₅H₂₁BF₂N₃S requires [M+H]⁺ 444.1512.

2.2.4. Synthesis of 3-(Benzo[d]Thiazol-2-yl)-6-Iodo-8-Phenyl-BODIPY (**3**)

To a solution of dye **TC497** (108 mg, 0.24 mmol) in DMF/methanol (MeOH) (1:1) (4.2 mL), a solution of iodine monochloride (124.7 mg, 0.77 mmol) in MeOH (2.5 mL) was added in 3 portions over 45 min. Upon completion of the reaction (monitored by TLC), DCM and water were added to the reaction mixture, and the organic phase was separated, washed with brine (2 × 50 mL), dried over anhydrous Na₂SO₄ and concentrated under reduced pressure. The residue was purified by FCC (elution system: DCM/PE 40–60 °C 4:6) to obtain compound **3** as an orange solid (98.3 mg, 72% yield). *R*_f: 0.93 (PE 40–60 °C/EtOAc 7:3); m.p. 134–136 °C; ¹H NMR (600 MHz, CDCl₃): δ 8.11 (d, *J* = 8.2 Hz, 1H), 7.95 (d, *J* = 8.0 Hz, 1H), 7.54–7.55 (m, 3H), 7.52–7.47 (m, 1H), 7.42 (t, *J* = 7.6 Hz, 1H), 7.33–7.32 (m, 2H), 7.13 (s, 1H), 2.75 (s, 3H), 1.46 (s, 3H), 1.45 (s, 3H); ¹³C NMR (75 MHz, CDCl₃): δ 160.2, 153.2, 147.3, 146.2, 143.1, 142.3, 137.3, 134.6, 133.6, 129.8, 129.7 (2C), 127.9 (2C), 126.5, 125.9, 124.1, 123.7, 121.7, 119.3, 114.2, 87.9, 17.3, 16.6, 14.8; HRMS (APCI⁺) Found: [M+H]⁺ 570.0482; molecular formula C₂₅H₂₀BF₂IN₃S requires [M+H]⁺ 570.0478.

2.2.5. General Procedure for the Suzuki Cross-Coupling Reaction towards Dyes **TC495**, **TC496** and **TC498**

To a solution of iodide **3** (1 eq) and the appropriate boronic acid (2 eq) in a mixture of toluene/ethanol/water 2:2:1 (0.01 M), K₂CO₃ (3 eq) was added, and the mixture was degassed and backfilled with argon. Pd(PPh₃)₄ (0.1 eq) was then added, and the mixture was degassed once again, backfilled with argon and refluxed upon completion of the reaction (~3 h). The reaction was then cooled to RT, H₂O was added, and the mixture was extracted with EtOAc. The combined organic layers were dried over anhydrous Na₂SO₄ and evaporated under reduced pressure. The residue was purified by FCC to afford the desired product.

2.2.6. Synthesis of 3-[(Benzo[d]Thiazol-2-yl)]-6-(2-Hydroxyphenyl)-8-Phenyl-BODIPY (**TC495**)

The title compound was obtained following the general procedure above for the Suzuki cross-coupling reaction using compound **3** (20 mg, 0.035 mmol) and 3-hydroxyphenyl boronic acid (9.7 mg, 0.07 mmol) after purification by FCC (elution system: DCM/MeOH 95:5) as a dark-purple solid (13.3 mg, 71% yield). *R*_f: 0.16 (DCM/MeOH 99:1); m.p. 305–307 °C (decomp.); ¹H NMR (600 MHz, CDCl₃): δ 8.21 (d, *J* = 8.1 Hz, 1H), 7.93 (d, *J* = 8.1 Hz, 1H), 7.56–7.52 (m, 4H), 7.43 (t, *J* = 7.5 Hz, 1H), 7.37–7.36 (m, 2H), 7.31 (bs, 1H), 7.28–7.25 (m, 1H), 6.82 (dd, *J* = 8.2, 1.8 Hz, 1H), 6.70 (d, *J* = 7.6 Hz, 1H), 6.63 (bs, 1H), 2.60 (s, 3H), 1.46 (s, 3H), 1.34 (s, 3H); ¹³C NMR (150 MHz, CDCl₃): δ 161.6, 159.3, 155.9, 150.8, 143.2, 143.1, 140.0, 136.4, 136.0, 134.6, 134.1, 134.0, 129.9, 129.7, 129.65 (2C), 128.0 (2C), 127.0, 126.1, 124.2, 122.8, 122.5, 121.7, 116.9, 115.0, 14.6, 14.3, 13.2; HRMS (APCI⁺) Found: [M+H]⁺ 536.1769; molecular formula C₃₁H₂₅ON₃BF₂S requires [M+H]⁺ 536.1774.

2.2.7. Synthesis 3-[(Benzo[d]Thiazol-2-yl)]-6-(4-Methoxyphenyl)-8-Phenyl-BODIPY (TC496)

The title compound was obtained following the general procedure above for the Suzuki cross-coupling reaction using compound **3** (15.8 mg, 0.03 mmol) and 4-methoxyphenyl boronic acid (9.1 mg, 0.06 mmol) after purification by FCC (elution system: hexane/DCM 1:1) as a pink-purple solid (8.6 mg, 52% yield). R_f : 0.30 (DCM/PE 40–60 °C 6:4); m.p. 280–282 °C, $^1\text{H NMR}$ (600 MHz, CDCl_3): δ 8.13 (d, $J = 8.4$ Hz, 1H), 7.93 (d, $J = 8.0$ Hz, 1H), 7.56–7.49 (m, 4H), 7.40 (t, $J = 7.6$ Hz, 1H), 7.37 (d, $J = 7.5$ Hz, 2H), 7.14 (bs, 1H), 7.08 (d, $J = 8.6$ Hz, 2H), 6.94 (d, $J = 8.6$ Hz, 2H), 3.83 (s, 3H), 2.61 (s, 3H), 1.46 (s, 3H), 1.35 (s, 3H); $^{13}\text{C NMR}$ (75 MHz, CDCl_3): δ 161.0, 159.2, 158.9, 153.9, 153.0, 149.7, 144.2, 142.9, 142.4, 140.0, 136.1, 134.9, 133.6, 131.2 (2C), 129.6 (2C), 128.1 (2C), 126.4, 125.6, 124.9, 123.5, 121.6, 116.2, 114.9, 114.1 (2C), 55.4, 14.6, 14.3, 13.2; HRMS (APCI⁺) Found: $[\text{M}+\text{H}]^+$ 550.1941; molecular formula $\text{C}_{32}\text{H}_{27}\text{BF}_2\text{N}_3\text{OS}$ requires $[\text{M}+\text{H}]^+$ 550.1930.

2.2.8. Synthesis 3-[(Benzo[d]Thiazol-2-yl)]-6-(3-Trifluoromethylphenyl)-8-Phenyl-BODIPY (TC498)

The title compound was obtained following the general procedure above for the Suzuki cross-coupling reaction using compound **3** (20 mg, 0.035 mmol) and 3-trifluoromethylphenyl boronic acid (13.3 mg, 0.07 mmol) after purification by FCC (elution system: PE 40–60 °C/DCM 6:4) as a dark pink solid (18.9 mg, 92% yield). R_f : 0.34 PE 40–60 °C/DCM 1:1; m.p. 214–216 °C, $^1\text{H NMR}$ (600 MHz, CDCl_3): δ 8.13 (d, $J = 8.2$ Hz, 1H), 7.95 (d, $J = 8.0$ Hz, 1H), 7.61 (d, $J = 7.8$ Hz, 1H), 7.50–7.58 (m, 5H), 7.36–7.43 (m, 5H), 7.16 (s, 1H), 2.61 (s, 3H), 1.49 (s, 3H), 1.35 (s, 3H); $^{13}\text{C NMR}$ (75 MHz, CDCl_3): δ 158.9, 158.5, 153.0, 145.6, 143.9, 142.3, 141.3, 137.1, 134.7, 134.3, 133.9, 133.5, 133.0, 131.2 (q, $J_{\text{CF}} = 32.4$ Hz), 129.6, 129.5 (2C), 129.2, 127.9 (2C), 127.5 (q, $J_{\text{CF}} = 269$ Hz), 126.9 (q, $J_{\text{CF}} = 3.7$ Hz), 126.5, 124.6 (q, $J_{\text{CF}} = 3.7$ Hz), 123.9, 123.6, 121.5, 118.5, 114.3, 14.7, 14.0, 13.1; HRMS (APCI⁺) Found: $[\text{M}+\text{H}]^+$ 588.1707; molecular formula $\text{C}_{32}\text{H}_{24}\text{BF}_5\text{N}_3\text{S}$ requires $[\text{M}+\text{H}]^+$ 588.1699.

2.2.9. Synthesis of 3,5-bis[(E)2-(Benzo[d]Thiazol-2-yl)Vinyl]-8-Phenyl-BODIPY (TC500)

To a solution of 8-phenyl-BODIPY (**1**) (30 mg, 0.09 mmol) in anhydrous DMF (0.6 mL), benzothiazole-2-carboxaldehyde (58.8 mg, 0.36 mmol), piperidine (3 drops) and acetic acid (3 drops) were added. The reaction mixture was stirred at 80 °C for 12 h. Upon completion of the reaction (monitored by TLC), the solvent was evaporated under reduced pressure, and the residue was purified by FCC (elution solvent: DCM) to afford **TC500** as a blue solid (6 mg, 10% yield). R_f : 0.22 (PE 40–60 °C/EtOAc 8:2); m.p. 248–250 °C; $^1\text{H NMR}$ (600 MHz, CDCl_3): δ 8.05 (d, $J = 7.4$ Hz, 2H), 8.03 (d, $J = 16.0$ Hz, 2H), 7.92 (d, $J = 7.8$ Hz, 2H), 7.58 (d, $J = 16.0$ Hz, 2H), 7.57–7.53 (m, 3H), 7.51 (t, $J = 7.4$ Hz, 2H), 7.43 (t, $J = 7.4$ Hz, 2H), 7.36–7.34 (m, 2H), 6.72 (bs, 2H), 1.49 (s, 6H); $^{13}\text{C NMR}$ (75 MHz, CDCl_3): δ 166.4, 154.0, 153.9, 151.3, 143.7, 141.5, 135.2, 134.5, 129.6, 129.5, 129.2, 128.1, 127.3, 126.7, 126.2, 123.5, 121.8, 119.4, 14.9; HRMS (APCI⁺) Found: $[\text{M}+\text{H}]^+$ 615.1647; molecular formula $\text{C}_{35}\text{H}_{26}\text{BF}_2\text{N}_4\text{S}$ requires $[\text{M}+\text{H}]^+$ 615.1655; Found: $[\text{M}+\text{Na}]^+$ 637.1470; molecular formula $\text{C}_{35}\text{H}_{25}\text{BF}_2\text{N}_4\text{NaS}_2$ requires $[\text{M}+\text{Na}]^+$ 637.1474.

2.2.10. Synthesis of 3-[(Benzo[d]Thiazol-2-yl)]-(E)-5-4-Iodostyryl)-8-Phenyl-BODIPY (**4**)

To a solution of dye **TC497** (79 mg, 0.18 mmol) in dry DMF (3.4 mL), 4-iodobenzaldehyde (82.7 mg, 0.36 mmol), piperidine (6 drops) and acetic acid (AcOH) (6 drops) were sequentially added. After 1 h, the reaction was complete (monitored by TLC), and the solvent was evaporated under reduced pressure. The residue was purified by FCC (elution system: PE 40–60 °C/EtOAc 9:1) to afford compound **4** as a purple solid (68.6 mg, 58% yield). R_f : 0.62 (PE 40–60 °C/EtOAc 8:2); m.p. 115–117 °C; $^1\text{H NMR}$ (600 MHz, CDCl_3): δ 8.12 (d, $J = 8.4$ Hz, 1H), 7.98 (d, $J = 8.0$ Hz, 1H), 7.78 (d, $J = 16.2$ Hz, 1H), 7.74 (d, $J = 8.3$ Hz, 2H), 7.57–7.50 (m, 4H), 7.44–7.41 (m, 1H), 7.37–7.35 (m, 2H), 7.27 (d, $J = 16.2$ Hz, 1H), 7.13 (d, $J = 8.3$ Hz, 2H), 7.12 (s, 1H), 6.72 (s, 1H), 1.49 (s, 3H), 1.48 (s, 3H); $^{13}\text{C NMR}$ (75 MHz, CDCl_3): δ 156.3, 153.2, 145.6, 144.9, 141.8, 140.5, 138.2, 138.0, 137.7 (2C), 135.6, 135.1, 134.7,

133.9, 131.1, 129.5 (2C), 129.0, 128.7, 128.2 (2C), 126.4, 125.7, 123.6, 123.4, 121.6, 119.6, 119.4, 110.2, 95.9, 14.8, 14.5; HRMS (APCI⁺) Found: [M+H]⁺ 658.0798; molecular formula C₃₂H₂₄BF₂IN₃S requires [M+H]⁺ 658.0791.

2.2.11. Synthesis of 3-[(Benzo[d]Thiazol-2-yl)]-5-[(E)-2-[Tert-Butyl(4-(Phenyl)prop-2-yn-1-yl)Carbamate]vinyl]-8-Phenyl-BODIPY (5)

To a solution of compound 4 (10.5 mg, 0.02 mmol) in Et₃N/benzene (1:1) (1 mL), *N*-BOC propargylamine (4.7 mg, 0.03 mmol) was added, followed by Pd(PPh₃)₄ (1.4 mg, 0.001 mmol). The reaction mixture was stirred at 80 °C. After 12 h, the reaction was complete (monitored by TLC), and the solvent was evaporated under reduced pressure. The residue was purified by FCC (elution solvent: DCM) to afford compound 5 as a purple solid (10 mg, 58% yield). *R*_f: 0.81 (DCM/MeOH 99:1); m.p. 230–232 °C (decomp.); ¹H NMR (300 MHz, CDCl₃): δ 8.11 (d, *J* = 7.3 Hz, 1H), 7.99 (d, *J* = 7.3 Hz, 1H), 7.77 (d, *J* = 16.0 Hz, 1H), 7.59–7.23 (m, 13H), 7.12 (s, 1H), 6.74 (s, 1H), 4.18 (bs, 2H), 1.59 (s, 3H), 1.48 (s, 12H); ¹³C NMR (75 MHz, CDCl₃): δ 160.0, 159.2, 158.7, 156.5, 155.4, 153.1, 145.6, 144.7, 141.6, 140.3, 138.4, 136.0, 135.3, 134.7, 132.3 (2C), 129.5 (2C), 128.2 (2C), 127.9 (2C), 126.4, 125.7, 124.0, 123.7, 123.5, 121.7, 119.8, 119.7, 110.1, 87.8, 83.2, 80.25, 29.9, 28.5, 22.8, 15.1, 14.6; HRMS (APCI⁺) Found: [M+H]⁺ 685.2614; molecular formula C₄₀H₃₆O₂N₄BF₂S requires [M+H]⁺ 685.2615.

2.2.12. Synthesis of 3-[(Benzo[d]Thiazol-2-yl)]-5-[(E)-2(4-(Phenyl)prop-2-yn-1-yl)Chloranimine]Vinyl]-8-Phenyl-BODIPY Hydrochloride (TC514)

Compound 5 (20 mg, 0.030 mmol) was dissolved in tetrahydrofuran (THF) (1 mL) containing 10% aqueous HCl solution (7.2 mL), and the reaction mixture was stirred at RT for 12 h. Upon completion of the reaction (monitored by TLC), the solvent was evaporated under reduced pressure. The residue was partitioned between diethyl ether (40 mL) and water, and the aqueous layer was extracted with diethyl ether (40 mL) and dried over anhydrous Na₂SO₄ and filtered. Dye TC514 fell out of the solution as a blue solid upon standing. The solid was filtered and dried under a high vacuum (10.0 mg, 54% yield). *R*_f: 0.58 (DCM/MeOH 8:2); m.p. 172–174 °C; ¹H NMR (600 MHz, CDCl₃): δ 8.15 (d, *J* = 8.1 Hz, 1H), 8.10 (d, *J* = 8.1 Hz, 1H), 7.77–7.56 (m, 11H), 7.44–7.43 (m, 2H), 7.11 (s, 1H), 7.08 (s, 1H), 4.08 (s, 2H), 1.53 (s, 3H), 1.47 (s, 3H); ¹³C NMR (150 MHz, CDCl₃/CD₃OD): δ 167.3, 158.8, 156.2, 152.8, 145.7, 144.1, 141.8, 140.4, 138.0, 136.8, 135.2, 134.4, 132.3 (2C), 129.5, 129.4 (2C), 128.0 (2C), 127.9 (2C), 126.4, 125.7, 123.4, 123.2, 122.1, 121.4, 119.9, 119.8, 110.0, 87.1, 81.6, 29.6, 14.8, 14.4; HRMS (APCI⁺) Found: [M]⁺ 585.2087; molecular formula C₃₅H₂₈N₄BF₂S requires [M]⁺ 585.2090.

2.2.13. Synthesis of 8-[(Benzo[d]Thiazol-2-yl)-BODIPY (6)

TFA (14 μL, 0.18 mmol) was added dropwise to a solution of benzothiazole-2-carboxaldehyde (300 mg, 1.8 mmol) and 2,4-dimethyl-1*H*-pyrrole (0.4 g, 4.6 mmol) in dry DCM (92 mL) at RT and the reaction mixture was stirred at the same temperature for 3 h. Then, the reaction was cooled to 0 °C with an ice bath, and a solution of DDQ (418 mg, 1.8 mmol) in dry DCM (62 mL) was added portion-wise over 1 h. The cooling bath was removed, the reaction was warmed to RT and Et₃N (3.7 mL, 30 mmol) was added, followed by the addition of BF₃·Et₂O (3.7 mL, 30 mmol) after 5 min. After stirring for 4 h, water (50 mL) was added to the reaction mixture. The organic layer was separated, diluted with DCM, washed with water (3 × 80 mL), dried over anhydrous Na₂SO₄, and concentrated under reduced pressure. The residue was purified by FCC (elution system: PE 40–60 °C/EtOAc 95:5) to afford compound 6 as an orange solid (68.6 mg, 10% yield). *R*_f: 0.46 (PE/EtOAc 9:1); m.p. 233–235 °C; ¹H NMR (600 MHz, CDCl₃): δ 8.17 (d, *J* = 8.0 Hz, 1H), 7.99 (d, *J* = 8.0 Hz, 1H), 7.60 (m, 1H), 7.53 (m, 1H), 6.02 (s, 2H), 2.57 (s, 6H), 1.51 (s, 6H); ¹³C NMR (75 MHz, CDCl₃): δ 160.7, 157.8, 153.1, 143.1, 136.2, 131.5, 131.1, 126.9, 126.5, 124.3, 122.0, 121.9, 14.9, 13.7; HRMS (APCI⁺) Found: [M+H]⁺ 382.1354; molecular formula C₂₀H₁₉N₃BF₂S requires [M+H]⁺ 382.1355.

2.2.14. Synthesis of 3,5-bis[(E)2-(Benzo[d]Thiazol-2-yl)Vinyl-8-[(Benzo[d]Thiazol-2-yl)-BODIPY (TC516)

To a solution of **6** (44.4 mg, 0.12 mmol) in dry DMF (2.4 mL), benzothiazole-2-carboxaldehyde (78.4 mg, 0.48 mmol), glacial AcOH (4 drops) and piperidine (4 drops) were added sequentially. The resulting mixture was heated at 72 °C. After 10 min, the reaction was complete (the color turned from reddish to dark green, indicating the completion of the reaction), and the reaction mixture was concentrated under reduced pressure. The residue was purified by FCC (elution system: DCM/Hexane/MeOH 90:10:0.5) to afford dye **TC516** as a light-green solid (9 mg, 11% yield). R_f : 0.30 (DCM/Hexane/MeOH 9:1:2 drops); m.p. 351–353 °C, ^1H NMR (600 MHz, CDCl_3): δ 8.21 (d, J = 8.1 Hz, 1H), 8.06 (d, J = 8.1 Hz, 2H), 8.04 (d, J = 8.0 Hz, 1H), 8.02 (d, J = 16.0 Hz, 2H), 7.93 (d, J = 7.9 Hz, 2H), 7.66–7.63 (m, 1H), 7.62 (d, J = 16.0 Hz, 2H), 7.59–7.55 (m, 1H), 7.51 (ddd, J = 8.1, 7.2, 1.3 Hz, 2H), 7.44 (ddd, J = 7.9, 7.2, 1.3 Hz, 2H), 6.77 (s, 2H), 1.63 (s, 6H); ^{13}C NMR (150 MHz, CDCl_3): δ 166.0, 160.0, 154.3, 153.1, 152.9, 143.3, 136.3, 135.4, 135.1, 130.5, 130.3, 127.2, 126.8, 126.3, 124.5, 124.1, 123.7, 122.1, 121.9, 119.9, 110.2, 14.1; HRMS (APCI⁺) Found: $[\text{M}+\text{H}]^+$ 672.1326; molecular formula $\text{C}_{36}\text{H}_{25}\text{N}_5\text{BF}_2\text{S}_3$ requires $[\text{M}+\text{H}]^+$ 672.1328.

2.3. Computational Studies

All DFT calculations have been performed using the Gaussian 16 software [49]. Geometry optimizations at the ground and excited states were conducted with the M06-2X functional and the 6-31G* basis set, using the polarized continuum model in the integral equation formalism (IEFPCM) [50] to include the solvation effect of ethanol. Spectroscopic properties were computed at the time-dependent DFT (TD-DFT) level using the CAM-B3LYP functional and the 6-31G* basis set. Further details of the calculations and justifications for the choice of functional and basis set can be found in the SI. Orbital visualizations were conducted using GaussView 5 [51].

2.4. Cellular Assays

2.4.1. Cell Culture

Mouse primary NIH/3T3 fibroblasts obtained from ATCC (Manassas, VA, USA) were cultured in high glucose Dulbecco's Modified Eagle's Medium (DMEM) supplemented with 10% Fetal bovine serum (FBS), 1% L-Glutamine and 1% Penicillin/Streptomycin at 37 °C and 5% CO_2 . Cells were seeded on 13 mm round glass coverslips pre-coated with a mixture of collagen (30 $\mu\text{g}/\text{mL}$) and gelatine (0.1% in ddH_2O) at a confluency of 10^4 cells/mL and allowed to attach and spread for 24 h prior to staining and imaging studies.

2.4.2. Fluorescence Stability and Cellular Toxicity

Cells were incubated in phenol-free OptiMEMTM I reduced serum medium with the different compounds diluted in 1% DMSO/PBS at concentrations of 0.1 μM , 1 μM and 10 μM at 37 °C in a humidified incubator under sterile conditions for 30 min, 90 min and 24 h. The morphology of living cells was examined under a light ZEISS AxioObserver Z1 microscope using a 10x/0.3NA dry lens. Then, cells were washed three times in PBS and fixed in 4% Paraformaldehyde (PFA)/PBS for 10 min. Nuclei were stained by incubating the cells in 1% DAPI/PBS solution for 5 min. Coverslips were mounted in glass slides with Mowiol/DABCO mounting medium and imaged using a LEICA SP8X WLL confocal system equipped with a 63x/1.4NA oil objective.

2.4.3. Cellular Biodistribution

NIH3T3 fibroblasts were seeded on 13 mm coverslips in DMEM medium supplemented with 10% FBS, 1% L-Glutamine and 1% Penicillin/Streptomycin at 37 °C and 5% CO_2 overnight, as described above. To examine the dye distribution in living cells, the different compounds diluted in 1% DMSO/PBS at concentrations of 0.1 μM , 1 μM and 10 μM were added to the cells in phenol-free OptiMEMTM I reduced serum medium and incubated for 15 min at 37 °C. After incubation, cells were washed three times in PBS,

fixed in 4% PFA for 10 min and mounted on glass slides with Mowiol/DABCO mounting medium. Images were acquired on a LEICA SP8X WLL confocal system using a 63x/1.4NA objective. To assess the dye staining in fixed cells, cells seeded in coverslips as above were washed three times with PBS and fixed with 4% PFA for 10 min without permeabilization. Fixed cells were incubated with the compounds at the working concentration determined in live cell imaging for 5 min, co-stained with 1% DAPI/PBS solution and mounted on glass slides with Mowiol/DABCO mounting medium.

For co-staining studies with endocytosis and lysosomal markers, NIH/3T3 fibroblasts seeded on coverslips were incubated with the indicated compounds at a working concentration in phenol-free OptiMEM™ I reduced serum medium for the indicated times at 37 °C. Cells were washed three times in PBS, fixed with 4% PFA for 10 min and permeabilized with 0.2% TritonX/PBS for 5 min at RT. Following blocking with 5% bovine serum albumin (BSA)/PBS for 1 h at RT, cells were incubated with goat anti-EEA1 early endosomal marker (abcam, cat no: ab206860, 1:200) and human anti-Lamp2 lysosomal marker (novus biologicals, cat no: NBP2-22217, 1:100) primary antibodies diluted in 1% BSA/PBS overnight at 4 °C. Following three washes with PBS, incubations with donkey anti-goat Alexa647, goat anti-mouse Alexa488 (Thermo Fischer, cat no A21447, 1:500, cat no A11017, 1:500) secondary antibody in 1% BSA/PBS were carried out for 1 h at RT. Nuclei were stained with 1% DAPI/PBS, and Mowiol/DABCO mounting medium was used to mount the coverslips in slides. Images were acquired on a LEICA SP8X WLL confocal system using a 63x/1.4NA objective.

2.4.4. Confocal and Lambda Scan Imaging

Confocal imaging was carried out on a LEICA SP8X WLL confocal system using the Argon laser for excitation at 488 nm and the White light laser for excitation at appropriate wavelengths. All images were acquired with a 63x/1.4NA oil objective and visualized with Leica LASX and Fiji Imaging software. Each compound was excited at the appropriate wavelength (exc), and emission light (em) was collected as follows:

TC496: exc 545 nm, em 555–700 nm

TC497: exc 535 nm, em 545–640 nm

TC498: exc 568 nm, em 577–640 nm

TC500: exc 610 nm, em 620–700 nm

TC514: exc 590 nm, em 598–700 nm

TC516: exc 635 nm, em 655–710 nm

For the co-staining experiments, detection of the EEA1 signals was achieved by excitation at 649 nm and emission collection at 658–700 nm. Lamp2 signal was detected by excitation at 647 and emission collection at 655–700 nm.

To determine the excitation wavelength that excites each compound best, we collected images in lambda mode, i.e., Λ scans for the best excitation wavelength and λ scan for the emission spectrum. Representative images and plots exported via LASX Leica software.

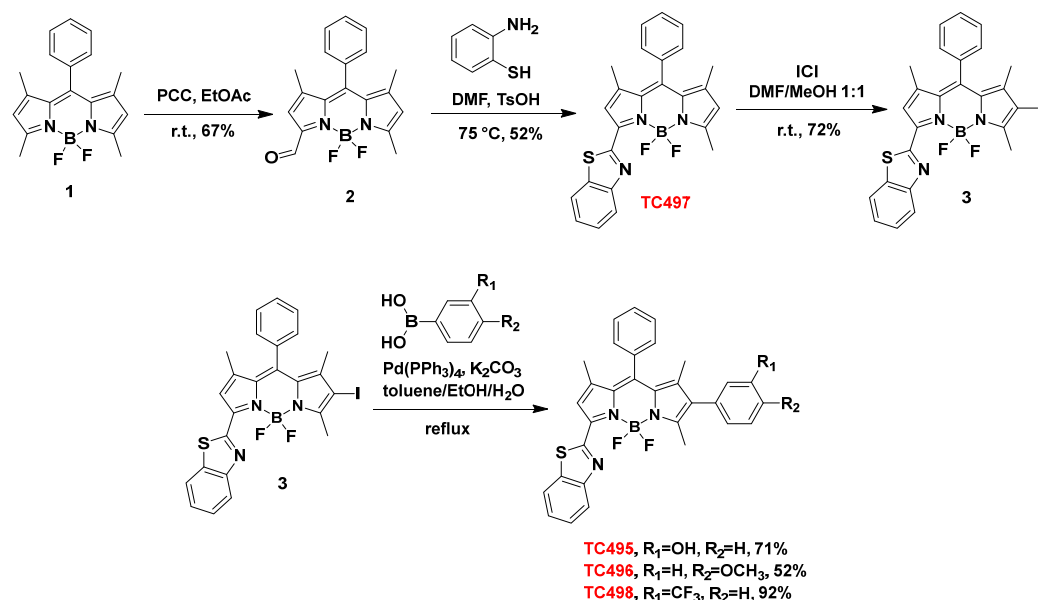
2.4.5. Time-Lapse Live Imaging

NIH3T3 fibroblasts were seeded on 8-well T/C treated ibidi imaging chamber slides pre-coated with 0.1% gelatin and 10 $\mu\text{g}/\text{mL}$ collagen I at a confluency of 10^4 per well in DMEM medium supplemented with 10% FBS, 1% L-Glutamine and 1% Penicillin/Streptomycin at 37 °C and 5% CO_2 . Following overnight incubation, the medium was changed to phenol-free OptiMEM™ I reduced serum medium, and the imaging chamber was transferred to the ZEISS AxioObserver Z1 microscope equipped with the live imaging chamber calibrated at 37 °C and 5% CO_2 . Image settings were set as follows: for **TC514** exc 583–600 nm reflector (92HE DAPI/GFP/mCherry), emis 617–758 nm, exposure time: 200 ms; for **TC498** exc 455–583 nm reflector (90HE DAPI/GFP/Cy3/Cy5), emis 579–604 nm and exposure time: 100 ms. Images were taken with zero intervals, using a 40x/1.3NA PinApo DICII oil lens. Compounds were added at time zero.

3. Results and Discussion

3.1. Chemistry

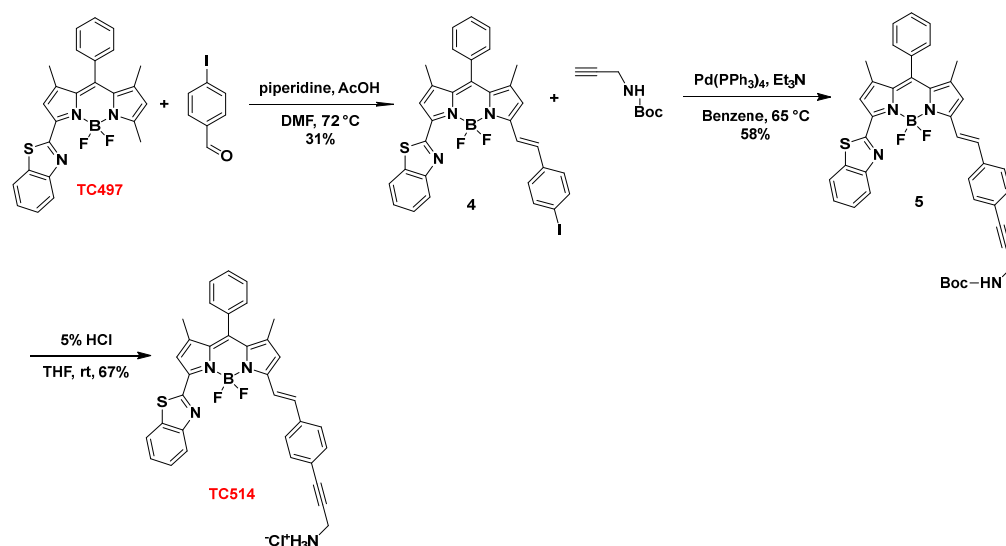
In the present study, we focused on the synthesis of a library of seven BZT-substituted BODIPYs with improved photophysical properties. Thus, modifications were carried out at the α , β and *meso* sites of 8-phenyl-BODIPY, aiming to further extend the π conjugation system across the BODIPY core (Figure 1). These changes induced a bathochromic shift of the absorption and emission maxima of the resulting dyes towards the red/near-infrared spectral range. Two modes of attachment of the BZT moiety on the BODIPY scaffold were envisioned (directly or via a styryl bridge) in combination with other aryl-substituted groups. In our effort to extend the π conjugation system, di- and tri-substituted analogs were also synthesized through a series of Knoevenagel condensations and carbon–carbon cross-coupling reactions such as Suzuki–Miyaura and Sonogashira reactions (Figure 4). Initially, the BZT group was introduced in 8-phenyl-BODIPY (**1**) at C3 (dye **TC497**). The reaction of **1** with PCC in EtOAc led to the mono-oxidation of the 3-methyl group to afford 3-formyl-8-phenyl-BODIPY (**2**) in 67% yield [52]. The aldehyde **2** was then reacted with 1,2-aminothiophenol in the presence of TsOH in anhydrous DMF at 72 °C to afford 3-benzothiazole-8-phenyl-BODIPY (**TC497**) in 52% yield [53] (Scheme 1). Subsequently, functionalization of **TC497** at C6 was pursued to investigate the effect of additional substituents at this position of the 8-phenyl-BODIPY scaffold. Thus, the introduction of an iodo substituent at C6 was affected by the reaction of **TC497** with iodide monochloride in a mixture of DMF/MeOH 1:1 at RT to afford **3** in 72% yield [54]. The position of the iodo group was confirmed by the disappearance of the signal corresponding to the C6 hydrogen in the ¹HNMR spectrum of **TC497**, resonating at 6.23 ppm. The iodide (**3**) was used as a key intermediate and participated in cross-coupling reactions to extend the π -conjugation across the BODIPY system. Iodide **3** underwent a Pd-catalyzed Suzuki–Miyaura coupling reaction [55] using *m*-hydroxy phenyl, *p*-methoxy phenyl, or *m*-(trifluoromethyl) phenylboronic acid in the presence of tetrakis(triphenylphosphine)palladium(0) as the catalyst and potassium carbonate as the base in a mixture of toluene/ethanol/water 3:1:1, to afford dyes **TC495** (71% yield), **TC496** (52% yield) and **TC498** (92% yield), respectively (Scheme 1).



Scheme 1. Synthesis of dyes **TC495–TC498**.

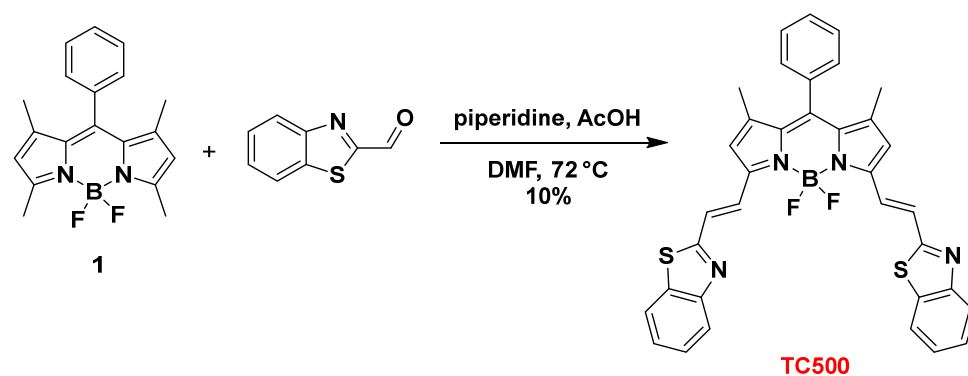
Subsequently, **TC497** was functionalized at C5 through the introduction of a substituted styryl moiety bearing an amino functionality as a hydrochloride salt to increase the aqueous solubility of the respective dye. Thus, Knoevenagel condensation [56] of **TC497** with *p*-iodo-benzaldehyde in the presence of piperidine and glacial acetic acid at 72 °C

led to compound **4** with a 31% yield. The *trans* stereochemistry of the vinyl group at C5 was confirmed by the coupling constant of the vinylic protons in the ^1H NMR spectrum resonating at 7.78 ppm (d, $J = 16.2$ Hz, 1H) and 7.27 ppm (d, $J = 16.2$ Hz, 1H). Then, the introduction of a *N*-BOC propargyl amine in **4** was effected via a Sonogashira cross-coupling reaction [57] using tetrakis(triphenylphosphine)palladium(0) as a catalyst in the presence of triethylamine in dry benzene at 65 °C to afford compound **5** in 58% yield. Treatment of **5** with 5% aq. HCl in THF at RT [58] led to the corresponding hydrochloride salt of dye **TC514** in a 67% yield (Scheme 2).



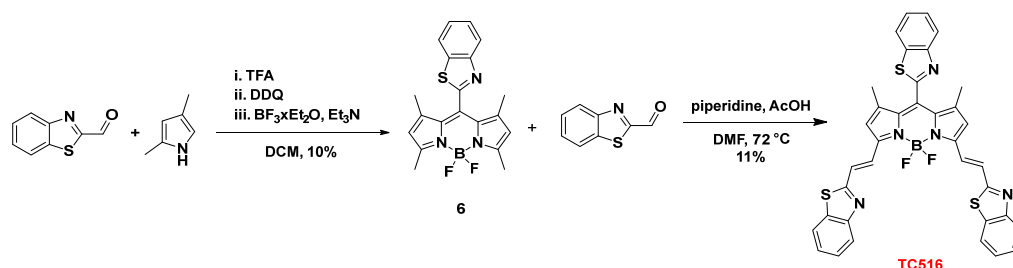
Scheme 2. Synthesis of dye **TC514**.

To further expand the structural diversity of our BZT-BODIPY derivatives, we introduced the BZT group through a vinyl spacer at positions C3 and C5 of 8-phenyl-BODIPY (**1**). Thus, Knoevenagel condensation of 8-phenyl-BODIPY (**1**) and benzothiazole-2-carboxaldehyde in the presence of piperidine and acetic acid in dry DMF at 72 °C afforded the symmetrical 3,5-disubstituted analog **TC500** albeit in low yield (10%) (Scheme 3).



Scheme 3. Synthesis of dye **TC500**.

Finally, the 8-BZT-substituted congener of the symmetric dye **TC500**, dye **TC516**, was prepared to explore the effect of the three BZT groups on the optical properties. Thus, benzothiazole-2-carboxaldehyde was reacted with 2,4-dimethyl pyrrole in the presence of TFA, followed by oxidation with DDQ and triethylamine-mediated boron chelation ($\text{BF}_3 \cdot \text{Et}_2\text{O}$) to afford 8-benzothiazolyl-BODIPY (**6**) (10% yield) [44]. Subsequently, the classical procedure for the Knoevenagel condensation, as previously described for the synthesis of dye **TC500**, yielded **TC516** in an 11% yield (Scheme 4). All the intermediates and final dyes were characterized by NMR spectroscopy and mass spectrometry (see Experimental Section in Supplementary Materials).



Scheme 4. Synthesis of dye **TC516**.

3.2. Optical Properties

The optical properties, along with the photophysical data of the new BZT-substituted BODIPY derivatives in ethanol (2×10^{-6} M), are summarized in Figures 5 and 6, Table 1 and Figures S22–S28 (ESI). 8-phenyl-BODIPY (**1**) was used as the control for comparison. In particular, the introduction of the BZT moiety directly attached at the C3 position red-shifted the maximum absorption wavelength of dye **TC497** by 42 nm and the maximum emission wavelength by 52 nm (λ_{abs} : 541 nm and λ_{emi} : 560 nm), displaying a high quantum yield ($\phi = 0.73$) significant molar extinction coefficient ($\epsilon = 54,400 \text{ M}^{-1}\text{cm}^{-1}$) and increased fluorescence lifetime ($\tau = 4.95$ ns). Considering the π -substituents at C6, dyes **TC495**, **TC496** and **TC498**, the maximum absorption and the emission peaks are shifted to longer wavelengths in comparison to **TC497** (Figure 5). Dye **TC496** bearing the electron donating (*p*-methoxy)phenyl substituent showed an enhanced bathochromic shift with $\lambda_{\text{emi}} = 605$ nm, with respect to the (*m*-trifluoromethyl)phenyl substituted **TC498** ($\lambda_{\text{emi}} = 580$ nm) and the (*m*-hydroxy)phenyl substituted **TC495** ($\lambda_{\text{emi}} = 586$ nm) (Figure 5). However, **TC496** possessed the lowest fluorescence quantum yield ($\phi = 0.01$) and molar extinction coefficient ($\epsilon = 16,600 \text{ M}^{-1}\text{cm}^{-1}$) among the C6-substituted dyes (Table 1). Thus, the introduction of an electron-donating group at the *meta* or *para* position of the C6-phenyl substituent induced a desirable bathochromic shift of the emission spectrum. However, these dyes possessed dramatically low quantum yields compared to that of **TC498**, bearing the electron-withdrawing CF_3 group at the *meta* position ($\phi = 0.56$ for **TC498**). Introduction of a styryl substituent at C5 of dye **TC497** (dye **TC514**) red-shifted both absorption and emission maxima above 600 nm, at 612 nm and 629 nm, respectively. Dye **TC514** has a relatively high fluorescence quantum yield ($\phi = 0.67$), high fluorescence lifetime ($\tau = 4.59$) and very good molar extinction coefficient ($\epsilon = 24,450 \text{ M}^{-1}\text{cm}^{-1}$). Moreover, **TC500** and **TC516**, substituted at C3 and C5 by a vinyl-BZT moiety, displayed an even higher bathochromic shift of the fluorescence towards the near-infrared centered at 656 nm and 677 nm, respectively (Figure 6). Furthermore, the replacement of the 8-phenyl group in **TC500** by the BZT moiety (dye **516**) shifted further the maximum emission wavelength by 21 nm ($\lambda_{\text{emi}} = 677$ nm). However, both **TC500** and **TC516** exhibited moderate fluorescence quantum yields ($\phi = 0.36$ and 0.31, respectively) and relatively small Stokes shifts of 9 nm and 7 nm, respectively.

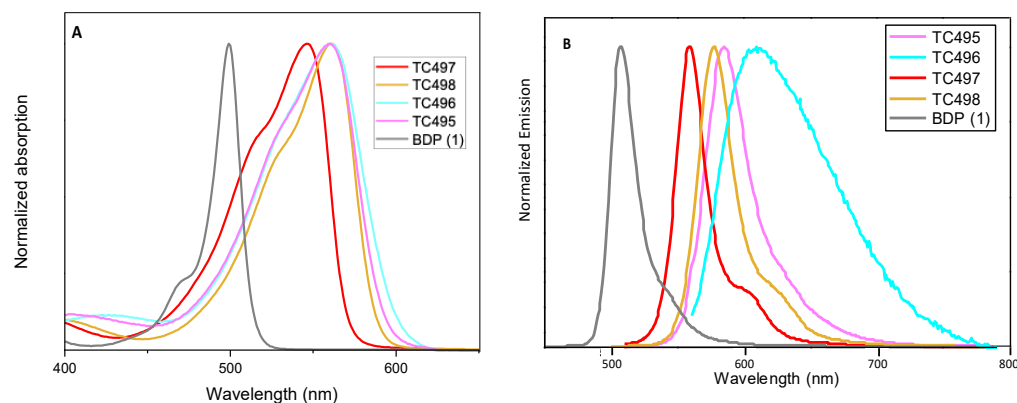


Figure 5. (A) UV-Vis electronic absorption spectra and (B) Photoluminescence spectra of solutions of dyes TC495–TC498 and the parent molecule 8-phenyl BODIPY (BDP) 1 in EtOH (concentration 2×10^{-6} M).

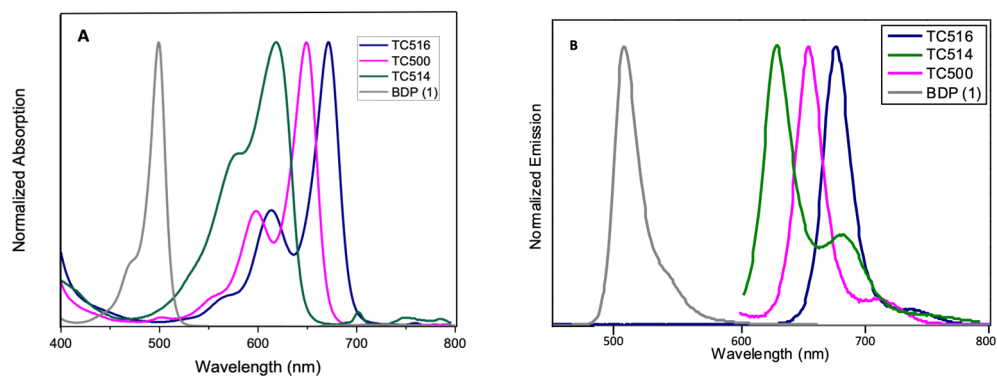


Figure 6. (A) UV-Vis electronic absorption spectra and (B) Photoluminescence spectra of solutions of dyes TC500, TC514 and TC516 and the parent molecule 8-phenyl BODIPY (BDP) 1 in EtOH (concentration 2×10^{-6} M).

Table 1. Spectroscopic properties of the new dyes in EtOH (2×10^{-6} M).

Dye	$\lambda_{\text{abs}}^{\text{a}}$ (nm)	$\lambda_{\text{em}}^{\text{b}}$ (nm)	$\Delta\lambda^{\text{c}}$ (nm)	$\Delta\nu$ (cm^{-1})	φ	Fluorescence Lifetime τ (ns)	ϵ ($\text{M}^{-1}\text{cm}^{-1}$)	Brightness ($\varphi \times \epsilon$)
1	499	508	9	355	0.61	3.5	55,500	33,850
TC495	555	586	31	954	0.11 ^d	1.58	97,800	10,758
TC496	555	605	50	1490	0.01 ^d	0.39	16,600	166
TC497	541	560	19	627	0.73 ^d	4.95	54,400	39,712
TC498	561	580	19	584	0.56 ^d	4.82	62,000	34,720
TC500	647	656	9	212	0.36 ^d	2.98	28,750	10,350
TC514	612	629	17	442	0.67 ^e	4.59	24,450	16,382
TC516	670	677	7	154	0.31 ^e	2.32	34,150	10,586

^a λ_{abs} = longest wavelength absorption maximum; ^b λ_{em} = fluorescence maximum, when excited at absorption maximum; ^c Computed from $\lambda_{\text{Stokes}} = \lambda_{\text{em}} - \lambda_{\text{abs}}$; ^d φ : fluorescence quantum yield was determined using rhodamine b as reference ($\varphi = 50\%$ in ethanol); ^e φ : fluorescence quantum yield was determined using cresyl violet as reference ($\varphi = 56\%$ in ethanol) [59].

3.3. Theoretical Calculations

(TD)DFT calculations (CAM-B3LYP/6–31G*) were performed to rationalize the spectroscopic properties of the newly synthesized derivatives (TC495, TC496, TC497, TC498, TC500, TC514 and TC516), together with 8-phenyl-BODIPY (1), which was used as a reference. The computed transition energies are in general agreement with the trends of

the experimental values, although they are systematically overestimated (see Table S1, ESI). The computed frontier molecular orbitals and energies are shown in Figure 7. For all the compounds, the HOMOs are delocalized over the whole molecule, except the substituent at the *meso*-position (phenyl for TC495, TC496, TC497, TC498, TC500, TC514 and 8-phenyl-BODIPY (1), benzothiazolyl for TC516). The LUMOs, on the other hand, are more localized on the central BODIPY structure, which indicates a charge redistribution from the conjugated substituents to the BODIPY core. The extended π -conjugation system of TC495, TC496, TC497, TC498, TC500 and TC514, as compared to 8-phenyl-BODIPY (1), leads to smaller HOMO-LUMO energy gaps, E_{HL} , and thus to smaller transition energies. The HOMO levels of the compounds with a benzothiazole substituent are only slightly changed in comparison with the parent molecule (1), while the ethenyl benzothiazole substituents at C3 and C5 of TC500 and TC516 led to a more pronounced destabilization of the HOMO levels, as well as a strong stabilization of the LUMO levels, which indicated a stronger interaction with the BODIPY core and led to the smallest transition energies thus, to even more red-shifted absorption and emission maxima among the seven molecules.

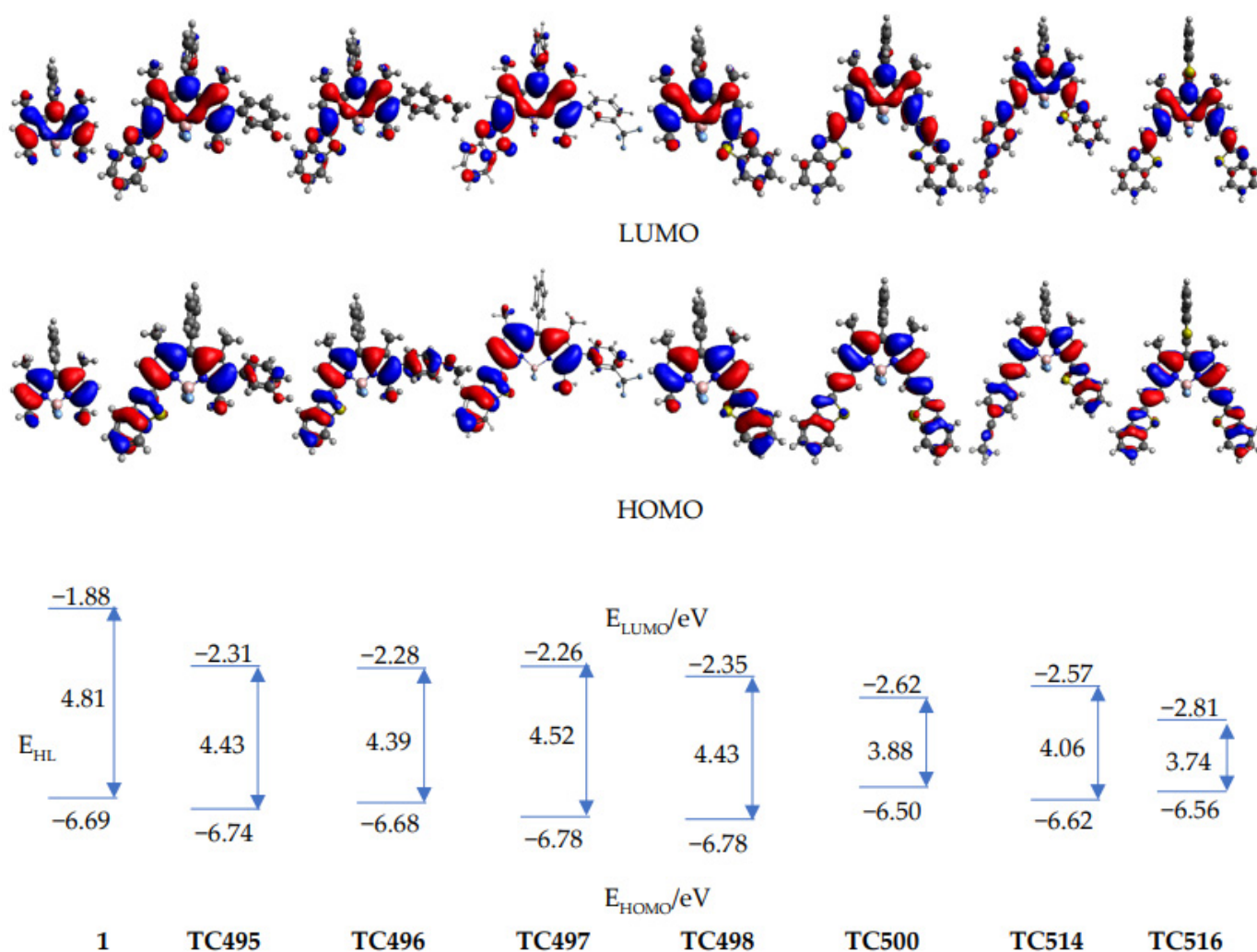


Figure 7. Frontier molecular orbital profiles of compounds 1, TC495–TC498, TC500, TC514 and TC516 and their energy levels, E_{HOMO} and E_{LUMO} ; E_{HL} denotes the energy difference between the frontier orbitals. All energies in eV.

It is interesting to consider the optimized structures of all the compounds in the ground and the first excited state. Steric interactions between the methyl groups at positions 1 and 7 force the phenyl group at position 8 of compounds TC495–TC498, TC500, TC514

and 8-phenyl BODIPY (**1**) in both states into a conformation far out of the BOPIPY plane (torsional angle $f_3 > 70^\circ$, see Figure 8); the bulkier benzothiazolyl group in **TC516** in the meso-position is fully perpendicular ($f_4 = 90^\circ$). Similarly, the 4-methoxy-phenyl group in **TC496**, the 3-hydroxy-phenyl group in **TC495** and the 3-trifluoromethyl-phenyl in **TC498** at position 6 are rotated out of the BODIPY plane to a substantial degree in both electronic states ($-50^\circ < f_2 < -40^\circ$), as is the benzothiazolyl group of compounds **TC495–TC498** and **TC514** in the ground state, although to a smaller extent ($f_1 = 20\text{--}28^\circ$). The ethenyl benzothiazole substituents in **TC500** and **TC516**, on the other hand, stay essentially planar both in S_0 and S_1 ($4^\circ < f_5 < 8^\circ$), and the nearly planar p -conjugated framework with large substituents is reflected in their small transition energies.

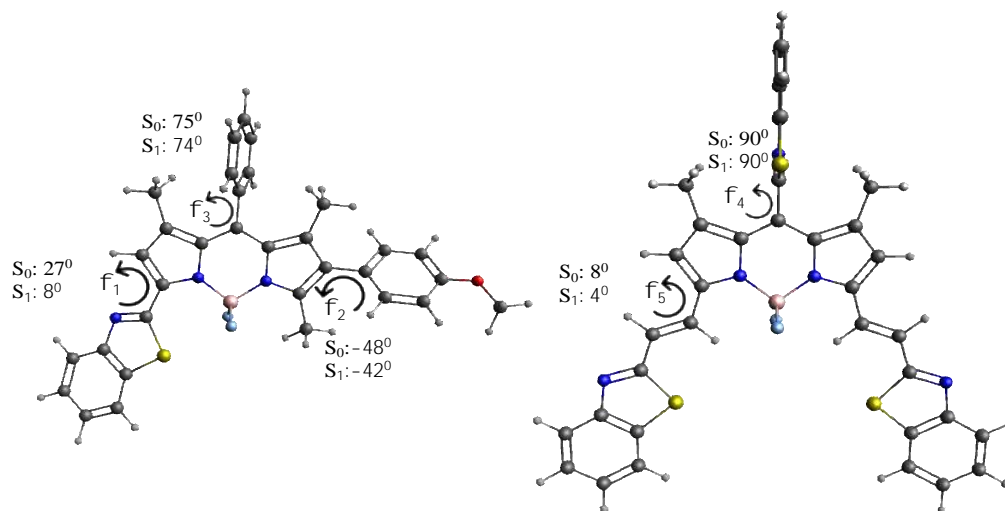


Figure 8. Selected dihedral angles of compounds **TC496** and **TC516** in the energy-optimized ground (S_0) and excited state (S_1).

Torsional angles $f_2\text{--}f_5$ do not change much in the relaxed excited state, although they are generally slightly smaller ($\sim 1\text{--}8^\circ$). Thus, they may not help to explain any trends in the Stokes shift. Torsional angle f_1 , on the other hand, decreases from $26\text{--}28^\circ$ in S_0 to $4\text{--}8^\circ$ in the relaxed excited state S_1 . This indicates that a substantial geometry relaxation takes place in compounds containing a 1,3-benzothiazolyl group during the transition from the vertically excited Franck–Condon state, where the geometry still coincides with that in S_0 , to the relaxed S_1 state, from which emission occurs. It has been shown [60] that an increased geometry relaxation in S_1 correlates with an increased Stokes shift. The geometry relaxation in S_1 is mainly determined by the change in the torsional angles describing the conformation of the large substituents, which explains why compounds with a benzothiazolyl substituent, i.e., **TC495**, **TC496**, **TC497**, and **TC514** show a larger Stokes shift than **TC500** and **TC516**, where no large scale geometry relaxation takes place (Table 1). We note that the quite large Stokes shift of compound **TC497** may have larger error margins due to the very small quantum yield of the compound ($\phi = 0.01$). We also note that much larger Stokes shifts associated with more substantial geometry relaxations in S_1 have been reported in Ref. [50]. Thus, this may serve as a criterion to design compounds with larger Stokes shifts in the future.

3.4. Cell Biodistribution

The cellular localization of the newly synthesized compounds was studied in cultured NIH3T3 mouse primary fibroblasts in both live and fixed conditions. To determine the minimum concentration that is effective for cell staining, cultured cells were incubated with the new dyes diluted in 1% DMSO in PBS for 15 min at three different concentrations (0.1 μM , 1 μM and 10 μM). After incubation, the cells were washed with PBS and fixed with paraformaldehyde (PFA) for 10 min. Nuclei were stained by DAPI. Images were acquired in

a confocal Leica SP8X WLL system at appropriate excitation wavelengths using the White Light Laser (WLL) and emission spectra. (Figure 9). The compound **TC495** did not stain cells in all concentrations tested (0.1 μM , 1 μM and 10 μM). In contrast, the compounds **TC496**, **TC497**, **TC498** and **TC500** efficiently labeled cells at a concentration of 1 μM , while **TC514** and **TC516** displayed effective staining at a much lower concentration of 0.1 μM . Given that most of the available BODIPY probes are used at concentrations of 2 μM [61], these dyes displayed improved sensitivity. All six dyes showed both diffuse and dotted localization patterns within the cell (Figure 9).

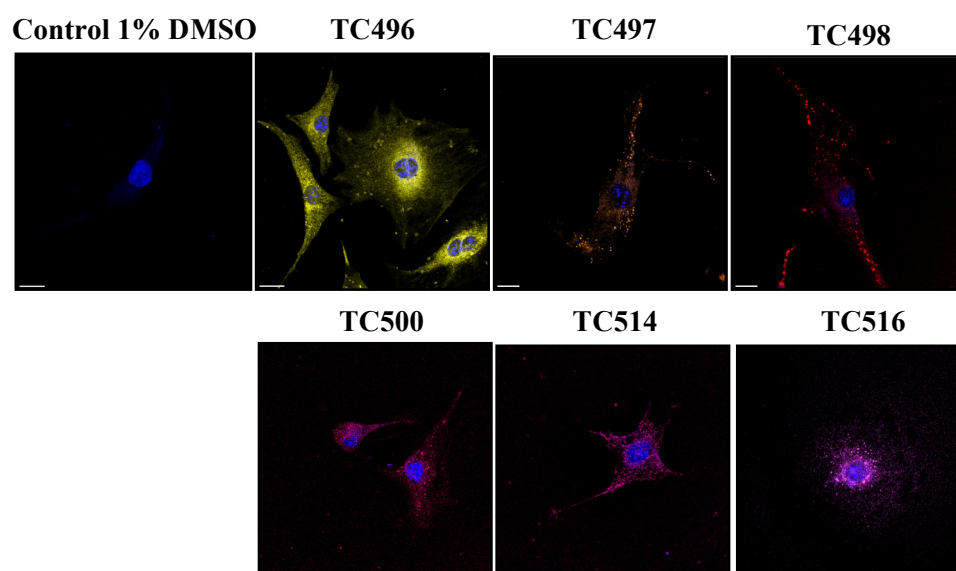


Figure 9. BODIPY probes localization. The new dyes were tested for their cellular localization in concentrations of 1 μM for **TC496**, **TC497**, **TC498** and **TC500** and 0.1 μM for **TC514** and **TC516**. Compounds were added to serum-free medium and incubated for 15 min at 37 °C. After incubation, cells were washed with PBS and fixed with PFA for 10 min. Images acquired in confocal Leica SP8 microscope. **TC496** is illustrated in yellow, **TC497** in orange, **TC498** in dark red, **TC500** in pink-red, **TC514** in pink and **TC516** in light purple color. Cell nuclei were stained by DAPI (in blue). Scale bars, 20 μm .

Subsequently, to assess the fluorescence stability and the toxicity of each of the new dyes (**TC495** was excluded, see above), fibroblasts were treated with the optimal concentrations for each BODIPY derivative (0.1 μM for **TC514** and **TC516** and 1 μM for **TC496**, **TC497**, **TC498** and **TC500**) for longer incubation times. The time points tested were 30 min, 90 min and 24 h (Figure S29, ESI). The pKa of **TC514** was calculated to be 8.55, using the program ChemAxon Marvin Beans v.14.9.29 [62]. Since the pH of the OptiMem™ cell medium and the PBS is ~7.4–7.6, the dye was tested as the hydrochloride salt. All six compounds tested at the optimal concentrations exhibited no toxic effects since no alteration in cell physiology was observed by imaging and were fluorescence stable at all time points even after 24 h incubation time.

Given the similar cell behavior of all six new BODIPY derivatives, we selected dye **TC514** to be further investigated because it exhibited efficient staining at a very low concentration (0.1 μM). First, we examined in detail the cellular localization of dye **TC514**. To assess whether it could stain the cell membrane, NIH3T3 fibroblasts were fixed for 10 min without permeabilization and then incubated with the dye for 5 min. **TC514** displayed diffuse staining in fixed fibroblasts, labeling mainly the cell membrane (Figure 10). Similar to the dotted pattern observed after 15 min incubation of **TC514** in living cells (Figure 9), 5 min incubation of **TC514** was sufficient to stain vesicular structures (Figure 10), indicating internalization of the dye. Live imaging from time zero after compound addition confirmed the aforementioned properties of **TC514**.

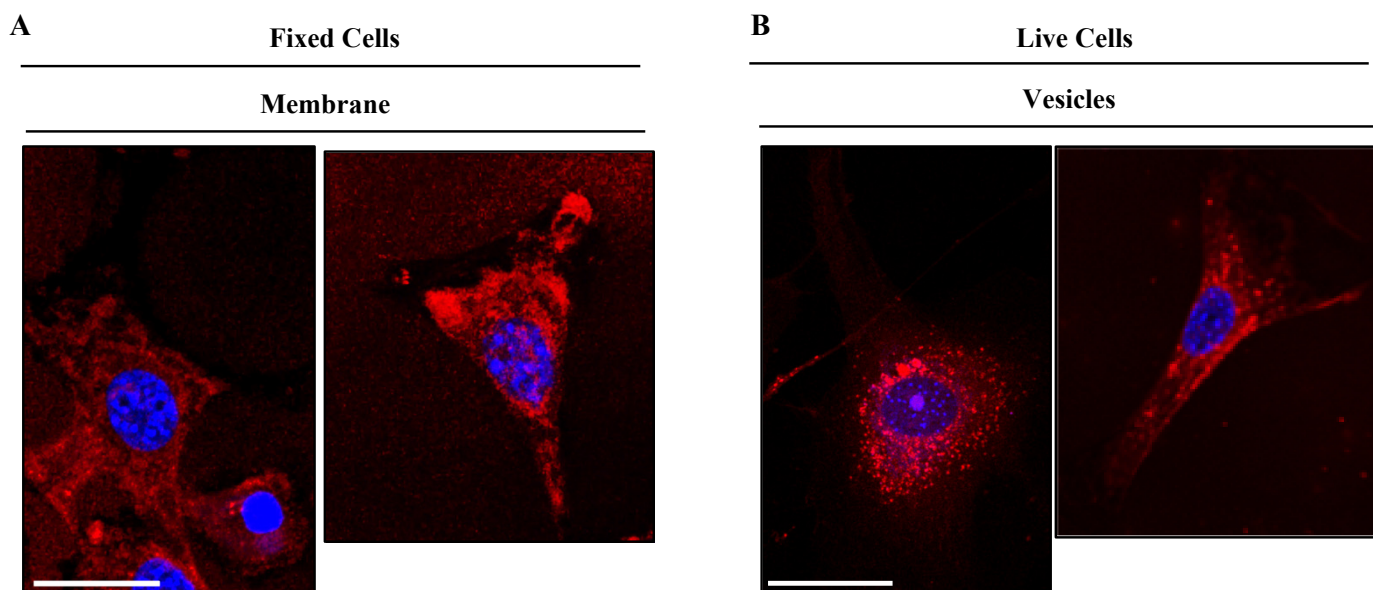


Figure 10. TC514 localization at the cell membrane and at subcellular vesicles. (A) TC514 was added in PFA-fixed cells for 5 min at 37 °C, cells washed and post-fixed for 10 min (B) TC514 was added in live cells for 5 min at 37 °C and then cells were washed with PBS and fixed with PFA for 10 min. Images acquired with confocal Leica SP8 microscope and illustrated in red color. The concentration used was 0.1 μ M. Cell nuclei were stained by DAPI (in blue). Scale bars, 10 μ m.

Driven by the previous results, we set out to identify the specific localization of TC514. TC514 bearing a propargyl ammonium group attached at the para position of the 5-styryl phenyl ring could probably act as a recognition moiety for lysosomes. Thus, we then performed a co-staining experiment with the Lamp2 lysosome marker. Cells were incubated with compound TC514 for 30 min to enable efficient trafficking of the dye to lysosomes, fixed with PFA, permeabilized in 0.2% Triton X100 and co-stained with anti-Lamp2 antibody. No staining of lysosomes was observed (Figure S30, ESI), as the fluorescence signal of TC514 did not co-localize with that of Lamp 2.

Moreover, we wanted to explore whether TC514 could be used as a co-staining dye in fluorescence microscopy experiments. For this reason, Λ capital scan for the excitation and λ scan were acquired using a confocal microscope to find the best excitation and emission wavelengths, respectively. Λ scan displayed a broad excitation spectrum with several “optimum” excitation peaks (490 nm, 580 nm, 590 nm) (Figure S31, ESI). Subsequently, emission spectra were acquired when the dye was excited at 488 nm or 405 nm. TC514 excited at 488 nm gave fluorescence staining, while when excited at 405 nm, it gave only background staining (Figure S32, ESI). These results suggest that TC514 has limited use for co-staining experiments because it cannot be used together with the most widely used fluorophores excited at 488 nm or 633 nm. However, it can be a useful marker of the cell membrane and could be exploited in live cell imaging experiments.

Finally, we investigated the specific cellular localization of compound TC498 based on its narrow emission peak observed in the lambda imaging scans. NIH3T3 fibroblasts were fixed with PFA for 10 min and then incubated with TC498 (1 μ M concentration) for 5 min without permeabilization. DAPI was used to stain the nuclei. Confocal imaging revealed a dotted localization pattern of TC498 in fixed cells, similar to living cell staining, indicating vesicular structures (Figure 11). These findings were further confirmed from live imaging from time zero after compound addition.

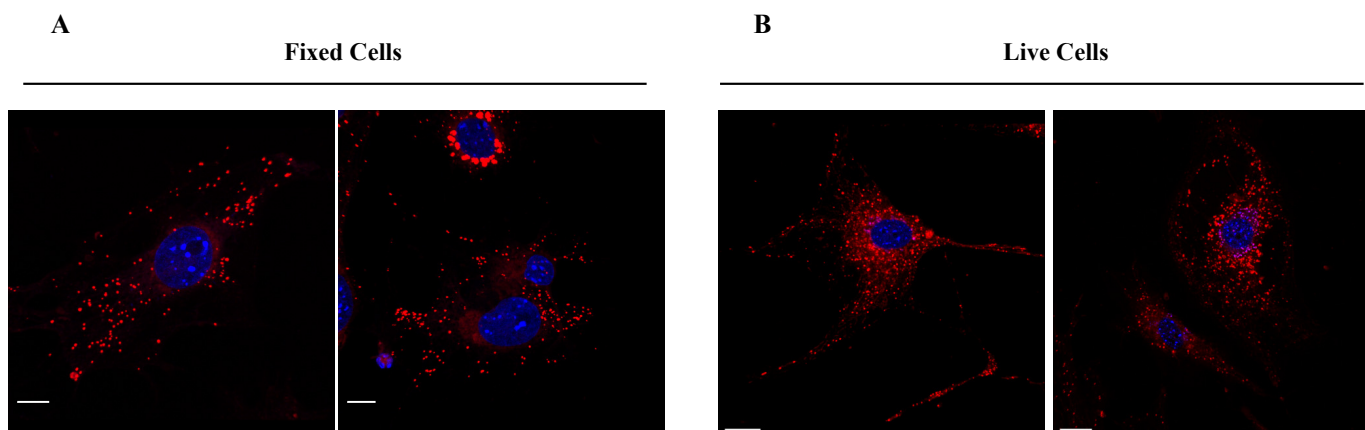


Figure 11. TC498 localization at cell membrane structures. (A) TC498 (1 μ M) was added to PFA fixed cells for 5 min at 37 $^{\circ}$ C, cells were washed and post-fixed for 10 min (B) TC498 (1 μ M) was added to live cells for 5 min at 37 $^{\circ}$ C and then cells were washed with PBS and fixed with PFA for 10 min. Images were acquired using a confocal Leica SP8 microscope and illustrated in red color. Cell nuclei were stained by DAPI (in blue). Scale bars, (A) 15 μ m, (B) 20 μ m.

Prompted by these results, we then intended to identify the intracellular trafficking of dye TC498. We examined whether TC498 could localize at early endosomes and lysosomes. Live cells were incubated with the dye for 5 min at 37 $^{\circ}$ C and subsequently permeabilized and stained with EEA1, which is a marker of early endosomes. No co-localization of the TC498 fluorescent signal at the early endosomes was observed (Figure 12).

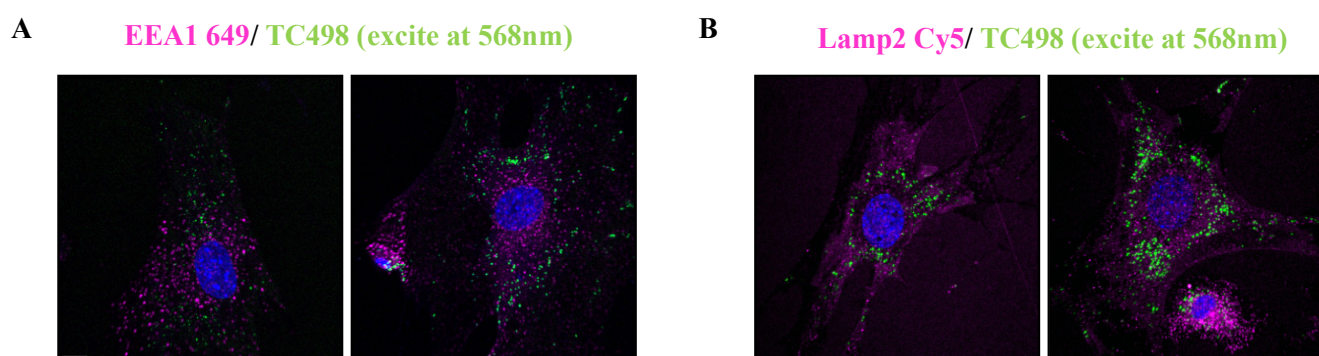


Figure 12. TC498 co-staining with endocytic vesicle markers. (A). TC498 added to live cells for 5 min at 37 $^{\circ}$ C, cells washed, fixed in PFA for 10 min and stained with immunofluorescence with EEA1 illustrated in magenta. (B) TC498 was added in live cells for 15 min at 37 $^{\circ}$ C, and then cells washed with PBS, fixed with PFA for 10 min and stained for Lamp2 in magenta in both TC498 is observed in green color. Images acquired in confocal Leica SP8 microscope. Cell nuclei were stained by DAPI (in blue). Scale bars, 10 μ m.

Then, live cells were incubated with the dye for 30 min at 37 $^{\circ}$ C before fixation, permeabilized and stained with Lamp2 lysosomal marker. The results showed that TC498 does not localize to lysosomes (Figure 12). Therefore, the dotted staining pattern could arise from association with specific cell membrane structures.

Next, we examined whether TC498 could be used as a co-staining dye. A capital scan and λ scan were performed in the confocal microscope. From the Λ scan, the best excitation wavelength for TC498 was at 568 nm. The scanning for the exact emission spectrum of the dye showed a specific emission peak at 584 nm when excited at 568 nm (Figure S32, ESI). To confirm that TC498 cannot emit at 488 nm or 405 nm and can be used as a co-staining marker, a lambda scan for TC498 was acquired when the dye was excited either at 488 nm or 405 nm. No signal other than background was observed at both wavelengths (Figure S33,

ESI). Conclusively, **TC498** could be used as a suitable marker for co-staining with dyes that are excited or emitting at 405, 488 or 633 nm.

4. Conclusions

In summary, we synthesized a library of novel BZT-substituted fluorophores based on the BODIPY platform. All the new dyes exhibited significant red-shifted absorption and emission maxima (ranging from 541 to 670 nm and 560 to 677 nm) compared to that of the parent 8-phenyl BODIPY (λ_{abs} : 499 nm, λ_{emi} : 508 nm), suitable Stokes shifts and moderate to high quantum yields. (TD)DFT calculations were carried out to corroborate the experimental spectroscopic findings through the investigation of electron distribution across the BODIPY core. Using fluorescence microscopy, we found that six out of the seven dyes efficiently stained mouse primary fibroblasts, namely **TC496**, **TC497**, **TC498** and **TC500** at a concentration of 1 μM , and **TC514** and **TC516** at a concentration of 0.1 μM . They showed both diffuse and dotted localization within the cell, with different staining patterns. The six dyes were non-toxic and fluorescently stable even after 24 h incubation of fibroblasts with the optimal dye concentration. Among them, **TC498** was found to be a new promising candidate that could be applied for co-staining protocols with dyes that are excited or emitting at 405, 488 or 633 nm.

Supplementary Materials: The following supporting information can be downloaded at <https://www.mdpi.com/article/10.3390/colorants3010002/s1>, Experimental section (general information): ^1H and ^{13}C NMR and HR-MS spectra of the final dyes **TC495**, **TC496**, **TC497**, **TC498**, **TC500**, **TC514** and **TC516**; optical data of dyes **TC495**, **TC496**, **TC497**, **TC498**, **TC500**, **TC514** and **TC516**; theoretical calculations, Table S1. Experimental and calculated absorption maxima λ_{abs} (in nm); oscillation strengths f in brackets. Photostability of dyes **TC496**, **TC497**, **TC498**, **TC500**, **TC514** and **TC516**, after long incubation; Staining profile of dyes **TC514** and **TC498**. References [63–73] are cited in the Supplementary Materials.

Author Contributions: Conceptualization, V.K., K.C.P. and T.C.; Funding acquisition, V.K. and T.C.; Methodology, O.K., C.A., H.R., V.K., K.C.P. and T.C.; Software, H.R.; Supervision, V.K., K.C.P. and T.C.; Validation, V.K., K.C.P. and T.C.; Writing—original draft, O.K., C.A. and H.R.; Writing—review and editing, V.K., K.C.P. and T.C. All authors have read and agreed to the published version of the manuscript.

Funding: This work was supported by the project BIOIMAGING-GR (Grant number MIS 5002755) implemented under “Action for Strengthening Research and Innovation Infrastructures”, funded by the Operational Programme “Competitiveness Entrepreneurship and Innovation” (NSRF 2014–2020) and co-financed by Greece and the European Union (European Regional Development Fund).

Institutional Review Board Statement: Not applicable.

Informed Consent Statement: Not applicable.

Data Availability Statement: Data will be made available on request.

Conflicts of Interest: The authors declare no conflicts of interest.

References

1. Cheng, H.-B.; Cao, X.; Zhang, S.; Zhang, K.; Cheng, Y.; Wang, J.; Zhao, J.; Zhou, L.; Liang, X.-J.; Yoon, J. BODIPY as a Multifunctional Theranostic Reagent in Biomedicine: Self-Assembly, Properties, and Applications. *Adv. Mater.* **2023**, *35*, 2207546. [[CrossRef](#)] [[PubMed](#)]
2. Gurubasavaraj, P.M.; Sajjan, V.P.; Muñoz-Flores, B.M.; Jiménez Pérez, V.M.; Hosmane, N.S. Recent Advances in BODIPY Compounds: Synthetic Methods, Optical and Nonlinear Optical Properties, and Their Medical Applications. *Molecules* **2022**, *27*, 1877. [[CrossRef](#)] [[PubMed](#)]
3. Antina, E.; Bumagina, N.; Marfin, Y.; Guseva, G.; Nikitina, L.; Sbytov, D.; Telegin, F. BODIPY Conjugates as Functional Compounds for Medical Diagnostics and Treatment. *Molecules* **2022**, *27*, 1396. [[CrossRef](#)] [[PubMed](#)]
4. Krämer, J.; Kang, R.; Grimm, L.M.; de Cola, L.; Picchetti, P.; Biedermann, F. Molecular Probes, Chemosensors, and Nanosensors for Optical Detection of Biorelevant Molecules and Ions in Aqueous Media and Biofluids. *Chem. Rev.* **2022**, *122*, 3459–3636. [[CrossRef](#)]

5. Kursunlu, A.N.; Bastug, E.; Guler, E. Importance of BODIPY-based Chemosensors for Cations and Anions in Bio-imaging Applications. *Curr. Anal. Chem.* **2020**, *18*, 163–175. [[CrossRef](#)]
6. Yan, M.; He, D.; Zhang, L.; Sun, P.; Sun, Y.; Qu, L.; Li, Z. Explorations into the meso-substituted BODIPY-based fluorescent probes for biomedical sensing and imaging. *Trends Anal. Chem.* **2022**, *157*, 116771. [[CrossRef](#)]
7. Li, F.Z.; Yin, J.F.; Kuang, G.C. BODIPY-based supramolecules: Construction, properties and functions. *Coord. Chem. Rev.* **2021**, *448*, 214157. [[CrossRef](#)]
8. Kowada, T.; Maeda, H.; Kikuchi, K. BODIPY-based probes for the fluorescence imaging of biomolecules in living cells. *Chem. Soc. Rev.* **2015**, *44*, 4953–4972. [[CrossRef](#)]
9. Zhang, Y.; Zheng, Y.; Meana, Y.; Raymo, F.M. BODIPYs with Photoactivatable Fluorescence. *Chem. Eur. J.* **2021**, *27*, 11257–11267. [[CrossRef](#)]
10. Nguyen, V.N.; Yim, Y.; Kim, S.; Ryu, B.; Swamy, K.; Kim, G.; Kwon, N.; Kim, C.Y.; Park, S.; Yoon, J. Molecular Design of Highly Efficient Heavy-Atom-Free Triplet BODIPY Derivatives for Photodynamic Therapy and Bioimaging. *Angew. Chem. Int. Ed.* **2020**, *59*, 8957–8962. [[CrossRef](#)]
11. Malacarne, M.C.; Gariboldi, M.B.; Caruso, E. BODIPYs in PDT: A Journey through the Most Interesting Molecules Produced in the Last 10 Years. *Int. J. Mol. Sci.* **2022**, *23*, 10198. [[CrossRef](#)]
12. Teng, K.-X.; Chen, W.-K.; Niu, L.-Y.; Fang, W.-H.; Cui, G.; Yang, Q.-Z. BODIPY-Based Photodynamic Agents for Exclusively Generating Superoxide Radical over Singlet Oxygen. *Angew. Chem. Int. Ed.* **2021**, *60*, 19912–19920. [[CrossRef](#)] [[PubMed](#)]
13. Kamkaew, A.; Lim, S.H.; Lee, H.B.; Kiew, L.V.; Chung, L.Y.; Burgess, K. BODIPY dyes in photodynamic therapy. *Chem. Soc. Rev.* **2013**, *42*, 77–88. [[CrossRef](#)] [[PubMed](#)]
14. Prieto-Montero, R.; Prieto-Castañeda, A.; Sola-Llano, R.; Agarrabeitia, A.R.; García-Fresnadillo, D.; López-Arbeloa, I.; Villanueva, A.; Ortiz, M.J.; de la Moya, S.; Martínez-Martínez, V.; et al. Exploring BODIPY Derivatives as Singlet Oxygen Photosensitizers for PDT. *Photochem. Photobiol.* **2020**, *96*, 458–477. [[CrossRef](#)] [[PubMed](#)]
15. Schneider, L.; Kalt, M.; Koch, S.; Sithamparanathan, S.; Villiger, V.; Mattiat, J.; Kradolfer, F.; Slyshkina, E.; Lubner, S.; Bonmarin, M.; et al. BODIPY-Based Photothermal Agents with Excellent Phototoxic Indices for Cancer Treatment. *J. Am. Chem. Soc.* **2023**, *145*, 4534–4544. [[CrossRef](#)] [[PubMed](#)]
16. Ni, Y.; Kannadorai, R.K.; Yu, S.W.-K.; Chang, Y.-T.; Wu, J. Push-Pull Type Meso-Ester Substituted BODIPY near-Infrared Dyes as Contrast Agents for Photoacoustic Imaging. *Org. Biomol. Chem.* **2017**, *15*, 4531–4535. [[CrossRef](#)] [[PubMed](#)]
17. Shi, Z.; Han, X.; Hu, W.; Bai, H.; Peng, B.; Ji, L.; Fan, Q.; Li, L.; Huang, W. Bioapplications of small molecule Aza-BODIPY: From rational structural design to in vivo investigations. *Chem. Soc. Rev.* **2020**, *49*, 7533–7567. [[CrossRef](#)] [[PubMed](#)]
18. Bodin, J.P.; Gateau, J.; Cois, J.; Lucas, T.; Lefebvre, F.; Moine, L.; Noiray, M.; Cailleau, C.; Denis, S.; Clavier, G.; et al. Biocompatible and Photostable Photoacoustic Contrast Agents as Nanoparticles Based on Bodipy Scaffold and Polylactide Polymers: Synthesis, Formulation, and In Vivo Evaluation. *ACS Appl. Mater. Interfaces* **2022**, *14*, 40501–40512. [[CrossRef](#)]
19. Lu, H.; Mack, J.; Yang, Y.; Shen, Z. Structural modification strategies for the rational design of red/nir region bodipys. *Chem. Soc. Rev.* **2014**, *43*, 4778–4823. [[CrossRef](#)]
20. Loudet, A.; Burgess, K. Bodipy Dyes and Their Derivatives: Syntheses and Spectroscopic Properties. *Chem. Rev.* **2007**, *107*, 4891–4932. [[CrossRef](#)]
21. Ulrich, G.; Ziessel, R.; Harriman, A. The chemistry of fluorescent bodipy dyes: Versatility unsurpassed. *Angew. Chem. Int. Ed.* **2008**, *47*, 1184–1201. [[CrossRef](#)]
22. Ziessel, R.; Ulrich, G.; Harriman, A. The chemistry of BODIPY: A new El Dorado for fluorescence tools. *N. J. Chem.* **2007**, *31*, 496–501. [[CrossRef](#)]
23. Yang, L.; Simionescu, R.; Lough, A.; Yan, H. Some observations relating to the stability of the BODIPY fluorophore under acidic and basic conditions. *Dyes Pigm.* **2011**, *91*, 264–267. [[CrossRef](#)]
24. Wang, M.; Vicente, M.G.H.; Mason, D.; Bobadova-Parvanova, P. Stability of a Series of BODIPYs in Acidic Conditions: An Experimental and Computational Study into the Role of the Substituents at Boron. *ACS Omega* **2018**, *3*, 5502–5510. [[CrossRef](#)] [[PubMed](#)]
25. Jameson, L.P.; Smith, N.W.; Annunziata, O.; Dzyuba, S.V. Interaction of BODIPY dyes with bovine serum albumin: A case study on the aggregation of a click-BODIPY dye. *Phys. Chem. Chem. Phys.* **2016**, *18*, 14182–14185. [[CrossRef](#)] [[PubMed](#)]
26. Karolin, J.; Johansson, L.B.-A.; Strandberg, L.; Ny, T. Fluorescence and Absorption Spectroscopic Properties of Dipyrrometheneboron Difluoride (BODIPY) Derivatives in Liquids, Lipid Membranes, and Proteins. *J. Am. Chem. Soc.* **1994**, *116*, 7801–7806. [[CrossRef](#)]
27. Li, G.; Li, J.; Otsuka, Y.; Zhang, S.; Takahashi, M.; Yamada, K. A BODIPY-Based Fluorogenic Probe for Specific Imaging of Lipid Droplets. *Materials* **2020**, *13*, 677. [[CrossRef](#)] [[PubMed](#)]
28. Liu, M.; Ma, S.; She, M.; Chen, J.; Wang, Z.; Liu, P.; Zhang, S.; Li, J. Structural modification of BODIPY: Improve its applicability. *Chin. Chem. Lett.* **2019**, *30*, 1815–1824. [[CrossRef](#)]
29. Cherumukkil, S.; Vedhanarayanan, B.; Das, G.; Praveen, V.K.; Ajayaghosh, A. Self-Assembly of Bodipy-Derived Extended π -Systems. *Bull. Chem. Soc. Jpn.* **2018**, *91*, 100–120. [[CrossRef](#)]
30. Gemen, J.; Ahrens, J.; Shimon, L.J.W.; Klajn, R. Modulating the Optical Properties of BODIPY Dyes by Noncovalent Dimerization within a Flexible Coordination Cage. *J. Am. Chem. Soc.* **2020**, *142*, 17721–17729. [[CrossRef](#)]

31. Blázquez-Moraleja, A.; Álvarez-Fernández, D.; Prieto Montero, R.; García-Moreno, I.; Martínez-Martínez, V.; Bañuelos, J.; Sáenz-de-Santa-María, I.; Chiara, M.D.; Chiara, J.L. A general modular approach for the solubility tagging of BODIPY dyes. *Dyes Pigm.* **2019**, *170*, 107545. [[CrossRef](#)]
32. Amendoeira, A.F.; Luz, A.; Valente, R.; Roma-Rodrigues, C.; Ali, H.; van Lier, J.E.; Marques, F.; Baptista, P.V.; Fernandes, A.R. Cell Uptake of Steroid-BODIPY Conjugates and Their Internalization Mechanisms: Cancer Theranostic Dyes. *Int. J. Mol. Sci.* **2023**, *24*, 3600. [[CrossRef](#)] [[PubMed](#)]
33. Romieu, A.; Massif, C.; Rihn, S.; Ulrich, G.; Ziessel, R.; Renarda, P.Y. The first comparative study of the ability of different hydrophilic groups to water-solubilise fluorescent BODIPY dyes. *N. J. Chem.* **2013**, *37*, 1016–1027. [[CrossRef](#)]
34. Boens, N.; Leen, V.; Dehaen, W. Fluorescent indicators based on bodipy. *Chem. Soc. Rev.* **2012**, *41*, 1130–1172. [[CrossRef](#)] [[PubMed](#)]
35. Wang, J.; Gong, Q.; Wang, L.; Hao, E.; Jiao, L. The main strategies for tuning BODIPY fluorophores into photosensitizers. *J. Porphyr. Phthalocyanines* **2020**, *24*, 603–635. [[CrossRef](#)]
36. Bañuelos, J. BODIPY Dye, the Most Versatile Fluorophore Ever? *Chem. Rec.* **2016**, *16*, 335–348. [[CrossRef](#)] [[PubMed](#)]
37. Ni, Y.; Wu, J. Far-red and near infrared BODIPY dyes: Synthesis and applications for fluorescent pH probes and bioimaging. *Org. Biomol. Chem.* **2014**, *12*, 3774–3791. [[CrossRef](#)] [[PubMed](#)]
38. Shing, W.; Law, C.; Yoon Yeong, K. Current trends of benzothiazoles in drug discovery: A patent review (2015–2020). *Expert. Opin. Ther. Pat.* **2022**, *32*, 299–315. [[CrossRef](#)]
39. Xuan, S.; Zhao, N.; Ke, X.; Zhou, Z.; Fronczek, F.R.; Kadish, K.M.; Smith, K.M.; Graca, M.; Vicente, H. Synthesis and Spectroscopic Investigation of a Series of Push-Pull Boron Dipyrromethenes (BODIPYs). *J. Org. Chem.* **2017**, *82*, 2545–2557. [[CrossRef](#)]
40. Henary, M.; Paranjpe, S.; Owens, E.A. Synthesis and applications of benzothiazole containing cyanine dyes. *Heterocycl. Commun.* **2013**, *19*, 1–11. [[CrossRef](#)]
41. Ren, M.; Wang, L.; Lv, X.; Liu, J.; Chen, H.; Wang, J.; Guo, W. Development of a benzothiazole-functionalized red-emission pyronin dye and its dihydro derivative for imaging lysosomal viscosity and tracking endogenous peroxynitrite. *J. Mater. Chem. B.* **2019**, *7*, 6181–6186. [[CrossRef](#)]
42. Aktan, E.; Uyar, T. Hetarylazopyrazolone Dyes Based on Benzothiazole and Benzimidazole Ring Systems: Synthesis, Spectroscopic Investigation, and Computational Study. *J. Chem.* **2017**, *2017*, 8659346. [[CrossRef](#)]
43. Das, S.; Indurthi, H.K.; Asati, P.; Saha, P.; Sharma, D.K. Benzothiazole based fluorescent probes for the detection of biomolecules, physiological conditions, and ions responsible for diseases. *Dyes Pigm.* **2022**, *199*, 110074. [[CrossRef](#)]
44. Shi, W.-J.; Chen, R.; Yang, J.; Wei, Y.-F.; Guo, Y.; Wang, Z.-Z.; Yan, J.-W.; Niu, L. Novel Meso-Benzothiazole-Substituted BODIPY-Based AIE Fluorescent Rotor for Imaging Lysosomal Viscosity and Monitoring Autophagy. *Anal. Chem.* **2022**, *94*, 14707–14715. [[CrossRef](#)] [[PubMed](#)]
45. Poronik, Y.M.; Yakubovskiy, V.P.; Shandura, M.P.; Vlasenko, Y.G.; Chernega, A.N.; Kovtun, Y.P. 3,5-Bis(benzothiazolyl)-Substituted BODIPY Dyes. *Eur. J. Org. Chem.* **2010**, *14*, 2746–2752. [[CrossRef](#)]
46. Sansalone, L.; Zhang, Y.; Mazza, M.M.A.; Davis, J.L.; Song, K.H.; Captain, B.; Zhang, H.F.; Raymo, F.M. High-Throughput Single-Molecule Spectroscopy resolves the conformational isomers of BODIPY chromophores. *J. Phys. Chem. Lett.* **2019**, *10*, 6807–6812. [[CrossRef](#)] [[PubMed](#)]
47. Prousis, K.C.; Canton-Vitoria, R.; Pagona, G.; Goulielmaki, M.; Zoumpourlis, V.; Tagmatarchis, N.; Calogeropoulou, T. New cationic heptamethinecyanine-graphene hybrid materials. *Dyes Pigment.* **2020**, *17*, 108047. [[CrossRef](#)]
48. Boens, N.; Verbelen, B.; Ortiz, M.J.; Jiao, L.; Dehaen, W. Synthesis of BODIPY dyes through postfunctionalization of the boron dipyrromethene core. *Coord. Chem. Rev.* **2019**, *399*, 213024. [[CrossRef](#)]
49. Frisch, M.J.; Trucks, G.W.; Schlegel, H.B.; Scuseria, G.E.; Robb, M.A.; Cheeseman, J.R.; Scalmani, G.; Barone, V.; Petersson, G.A.; Nakatsuji, H.; et al. *Gaussian 16*; Revision B.01; Gaussian Inc.: Wallingford, CT, USA, 2016.
50. Tomasi, J.; Mennucci, B.; Cammi, R. Quantum mechanical continuum solvation models. *Chem. Rev.* **2005**, *105*, 2999–3093. [[CrossRef](#)]
51. Dennington, R.; Keith, T.A.; Millam, J.M. *GaussView 5.0*; Semichem Inc.: Shawnee Mission, KS, USA, 2016.
52. Ramos-Torres, Á.; Avellanal-Zaballa, E.; Prieto-Castañeda, A.; García-Garrido, F.; Bañuelos, J.; Agarrabeitia, A.R.; Ortiz, M.J. Formyl BODIPYs by PCC-Promoted Selective Oxidation of α -MethylBODIPYs. Synthetic Versatility and Applications. *Org. Lett.* **2019**, *21*, 4563–4566. [[CrossRef](#)]
53. Kaur, G.; Moudgil, R.; Shamim, M.; Gupta, V.K.; Banerjee, B. Camphor sulfonic acid catalyzed a simple, facile, and general method for the synthesis of 2-arylbenzothiazoles, 2-arylbenzimidazoles, and 3H-spiro[benzo[d]thiazole-2,3'-indolin]-2'-ones at room temperature. *Synth. Commun.* **2021**, *51*, 1100–1120. [[CrossRef](#)]
54. Wang, J.B.; Fang, X.Q.; Pan, X.; Dai, S.Y.; Song, Q.H. New 2,6-Modified Bodipy Sensitizers for Dye-Sensitized Solar Cells. *Chem. Asian J.* **2012**, *7*, 696–700. [[CrossRef](#)] [[PubMed](#)]
55. Huang, L.; Cui, X.; Therrien, B.; Zhao, J. Energy-Funneling-Based Broadband Visible-Light-Absorbing Bodipy-C₆₀ Triads and Tetrads as Dual Functional Heavy-Atom-Free Organic Triplet Photosensitizers for Photocatalytic Organic Reactions. *Chem. Eur.* **2013**, *19*, 17472–17482. [[CrossRef](#)]
56. Huang, L.; Yu, X.; Wu, W.; Zhao, J. Styryl Bodipy-C₆₀ Dyads as Efficient Heavy-Atom-Free Organic Triplet Photosensitizers. *Org. Lett.* **2012**, *14*, 2594–2597. [[CrossRef](#)] [[PubMed](#)]

57. Yang, P.; Zhao, J.; Wu, W.; Yu, X.; Liu, Y. Accessing the Long-Lived Triplet Excited States in Bodipy-Conjugated 2-(2-Hydroxyphenyl) Benzothiazole/Benzoxazoles and Applications as Organic Triplet Photosensitizers for Photooxidations. *J. Org. Chem.* **2012**, *77*, 6166–6178. [[CrossRef](#)] [[PubMed](#)]
58. Erten-Ela, S.; Yilmaz, M.D.; Icli, B.; Dede, Y.; Icli, S.; Akkaya, E.U. A panchromatic boradiazaindacene (BODIPY) sensitizer for dye-sensitized solar cells. *Org. Lett.* **2008**, *10*, 3299–3302. [[CrossRef](#)] [[PubMed](#)]
59. Brouwer, A.M. Standards for photoluminescence quantum yield measurements in solution (IUPAC Technical Report). *Pure Appl. Chem.* **2011**, *83*, 2213–2228. [[CrossRef](#)]
60. Chen, Y.; Zhao, J.; Guo, H.; Xie, L. Geometry Relaxation-Induced Large Stokes Shift in Red-Emitting Borondipyrromethenes (BODIPY) and Applications in Fluorescent Thiol Probes. *J. Org. Chem.* **2012**, *77*, 2192–2206. [[CrossRef](#)]
61. Bittel, A.M.; Davis, A.M.; Wang, L.; Nederlof, M.A.; Escobedo, J.O.; Strongin, R.M.; Gibbs, S.L. Varied Length Stokes Shift BODIPY-Based Fluorophores for Multicolor Microscopy. *Sci. Rep.* **2018**, *8*, 4590. [[CrossRef](#)]
62. Marvin 14.9.29, ChemAxon. 2014. Available online: <http://www.chemaxon.com> (accessed on 1 January 2023).
63. Würth, C.; Grabolle, M.; Pauli, J.; Spieles, M.; Resch-Genger, U. Relative and absolute determination of fluorescence quantum yields of transparent samples. *Nat. Protoc.* **2013**, *8*, 1535–1550. [[CrossRef](#)]
64. Chibani, S.; Laurent, A.D.; Le Guennic, B.; Jacquemin, D. Improving the Accuracy of Excited-State Simulations of BODIPY and Aza-BODIPY Dyes with a Joint SOS-CIS(D) and TD-DFT Approach. *J. Chem. Theory Comput.* **2014**, *10*, 4574–4582. [[CrossRef](#)] [[PubMed](#)]
65. Chibani, S.; Le Guennic, B.; Charaf-Eddin, A.; Maury, O.; Andraud, C.; Jacquemin, D. On the Computation of Adiabatic Energies in Aza-Boron-Dipyrromethene Dyes. *J. Chem. Theory Comput.* **2012**, *8*, 3303–3313. [[CrossRef](#)] [[PubMed](#)]
66. Chibani, S.; Le Guennic, B.; Charaf-Eddin, A.; Laurent, A.D.; Jacquemin, D. Revisiting the optical signatures of BODIPY with ab initio tools. *Chem. Sci.* **2013**, *4*, 1950–1963. [[CrossRef](#)]
67. Yanai, T.; Tew, D.P.; Handy, N.C. A new hybrid exchange–correlation functional using the Coulomb-attenuating method (CAM-B3LYP). *Chem. Phys. Lett.* **2004**, *393*, 51–57. [[CrossRef](#)]
68. Martin, R.L. Natural Transition Orbitals. *J. Chem. Phys.* **2003**, *118*, 4775–4777. [[CrossRef](#)]
69. Ngoy, B.P.; Molupe, N.; Harris, J.; Fomo, G.; Mack, J.; Nyokong, T. Photophysical studies of 2,6-dibrominated BODIPY dyes substituted with 4-benzyloxystyryl substituents. *J. Porphyr. Phtalocyanines* **2017**, *21*, 431–438. [[CrossRef](#)]
70. Ghai, L.; Mack, J.; Lu, H.; Yamada, H.; Kuzuhara, D.; Lai, G.; Li, Z.; Shen, Z. New 2,6-Distyryl-Substituted BODIPY Isomers: Synthesis, Photophysical Properties, and Theoretical Calculations. *Chem. Eur. J.* **2014**, *20*, 1091–1102. [[CrossRef](#)]
71. Ni, Y.; Zeng, L.; Kang, N.-Y.; Huang, K.-W.; Wang, L.; Zeng, Z.; Chang, Y.-T.; Wu, J. meso-Ester and Carboxylic Acid Substituted BODIPYs with Far-Red and Near-Infrared Emission for Bioimaging Applications. *Chem. Eur. J.* **2014**, *20*, 2301–2310. [[CrossRef](#)]
72. Momeni, M.R.; Brown, A. Why do TD-DFT excitation energies of BODIPY/Aza-BODIPY families largely deviate from experiment? Answers from electron correlated and multireference methods. *J. Chem. Theory Comput.* **2015**, *11*, 2619–2632. [[CrossRef](#)]
73. Postils, V.; Ruiperez, F.; Casanova, D. Mild Open-Shell Character of BODIPY and Its Impact on Singlet and Triplet Excitation Energies. *J. Chem. Theory Comput.* **2021**, *17*, 5825–5838. [[CrossRef](#)]

Disclaimer/Publisher’s Note: The statements, opinions and data contained in all publications are solely those of the individual author(s) and contributor(s) and not of MDPI and/or the editor(s). MDPI and/or the editor(s) disclaim responsibility for any injury to people or property resulting from any ideas, methods, instructions or products referred to in the content.